

RETURNING MATERIALS:
Place in book drop to remove this checkout from your record. FINES will be charged if book is returned after the date stamped below.

GRAIN BOUNDARY MIGRATION AND DYNAMIC RECRYSTALLIZATION OF NICKEL DURING HIGH TEMPERATURE LOW CYCLE FATIGUE

Вy

Shuhrong Chen

A THESIS

Submitted to

Michigan State University

in partial fulfillment of the requirements

for the degree of

MASTER OF SCIENCE

Department of Metallurgy, Mechanics and Materials Science

ABSTRACT

GRAIN BOUNDARY MIGRATION AND DYNAMIC RECRYSTALLIZATION
OF NICKEL DURING HIGH TEMPERATURE LOW CYCLE FATIGUE

Вy

Shuhrong Chen

Microstructural developments of Ni polycrystals during high temperature low cycle fatigue were studied. Extensive grain boundary migration and dynamic recrystallization were observed. Dynamic recrystallization can be initiated at a drastically lower stress value during cyclic deformation at large cumulative strains than in monotonic tests. A total strain amplitude as small as 0.375% was found sufficient to set off dynamic recrystallization in Ni polycrystals during low cycle fatigue at high temperature, and there is circumstantial evidence that dynamic recrystallization is the major softening mechanism. The microstructural investigations suggest that recrystallization twinning and grain boundary bulging may be responsible for the nucleation of dynamic recrystallization during low cycle fatigue.

ACKNOWLEDGEMENTS

First and foremost, I would like to thank my advisor, Professor G. Gottstein, for his patient guidance and beneficial discussions in making this project a success. Also, I would like to express my deepest gratitude to my mother and my parents-in-law for their boundless love and full support. The considerateness, understanding and encouragement coming from my wife, Bihling, made everything go smoothly. I would also like to thank my friends in the MMM department, for teaching me experimental techniques and conveying their experience.

Finally, the support of the U.S. Department of Energy, Office of Basic Science, under grant number DE-FG02-85ER 45205 is gratefully acknowledged.

TABLE OF CONTENTS

		Pag
LIST	OF TABLES	iv
LIST	OF FIGURES	v
I	INTRODUCTION	1
II	LITERATURE SURVEY	
	2.1 Grain Boundary Migration During LCF	3
	2.2 DRX In Monotonic Tests	4
	2.3 DRX During LCF	9
III	EXPERIMENTAL PROCEDURE	
	3.1 Testing Materials	11
	3.2 Specimens Preparation	11
	3.2.1 Mechanical Testing Specimens	11
	3.2.2 Optical Microscopy Specimens	14
	3.2.3 Electron Microscopy Specimens	14
	3.3 Mechanical Testing	15
	3.4 The Microhardness Test	18
IV	EXPERIMENTAL RESULTS	
	4.1 Mechanical Behavior	19
	4.2 Microstructural Development	25
	4.3 Evidence Of DRX Under LCF	34
	4.4 Dislocation Structures	43
	4.5 Result Of A Cu Single Crystal	47
v	DISCUSSIONS	50
VI	CONCLUSIONS	5 5
VII	REFERENCES	57

LIST OF TABLES

Tab	ole	Page
1.	Composition of Ni studied	11
2.	Composition of Al studied	11
3.	Jet polishing conditions for Ni and Al	15
4.	Hardness distribution in Fig. 22	41

LIST OF FIGURES

		Figure Captions	Page
Fig.	1.	True resolved shear stress vs. true resolved shear strain	
		for <111> Ni single crystal [6].	5
Fig.	2.	Flow curves of a plain 0.25% C steel in the austenite	
		state (fcc) at 1100° C (0.76 $T_{\rm m}$), illustrating the strong	
		influence of strain rate [27].	8
Fig.	3.	Geometry and dimensions of testing samples.	13
Fig.	4.	Gauge sectional geometry and orientation of the Cu single	
		crystal.	13
Fig.	5.	Arrangement of the high temperature mechanical testing	
		setup.	17
Fig.	6.	True stress amplitude vs. cumulative strain of Ni with	
		1% total strain amplitude.	20
Fig.	7.	True stress amplitude vs. cumulative strain of Ni with	
		0.5% total strain amplitude.	21
Fig.	8.	True stress amplitude vs. cumulative strain of Ni with	
		0.375% total strain amplitude.	22
Fig.	9.	True stress amplitude vs. cumulative strain of Al with	
		0.5% total strain amplitude.	23
Fig.	10.	True stress amplitude vs. cumulative strain of a Cu	
		single crystal with 1% total strain amplitude.	24
Fig.	11.	The microstructure of Ni after annealing at 800 C for	
		5 hours.	26
Fig.	12.	The microstructure of Ni after 200 cycles with 0.5%	
		total strain amplitude at 600 C.	26

Fig. 3	13.	The microstructures of Ni in a plane parallel to the	
		loading direction after cyclic deformation with 0.5%	
		strain amplitude at 600 °C (a) Annealed at 800 °C for 5	
		hours; (b) after 10 complete cycles at 600 °C, slightly	
		polished and etched again to reveal the new grain boundary	
		positions; (c) right after 10 complete cycles, positions A,	
		B,C and D indicate inhomogeneous strain distribution on	
		the surface; (d) etched to reveal the positions of new	
		and original grain boundaries simultaneously; (e) right	
		after 40 cycles; (f) the positions of new and original	
		grain boundaries after etching again; (g) slightly	
		polished and etched again, only new grain boundaries can	
		be seen; (h) right after 160 cycles; (i) after etching;	
		(j) after polishing and etching.	28
Fig.	14.	Detailed structure of a surface marking after 10 cycles.	32
Fig.	15.	The microstructure of Al (a) after annealing at 310 °C	
		for 5 hours; (b) after 720 cycles with 0.5% total strain	
		amplitude at 200°C. The two figures are not taken from	
		the same area.	32
Fig.	16.	Serrations of a grain boundary in Ni after 200 cycles	
		with 0.5% total strain amplitude.	35
Fig.	17.	A protrusion and a new grain at a grain boundary in Ni	
		after 200 cycles with 0.5% total strain amplitude.	35
Fig.	18.	A new grain on the grain boundary in Ni after 510 cycles	
		with 0.5% total strain amplitude.	36

	Figure Captions	Page
Fig. 19.	A new grain formed at a twin boundary in Ni after 200	
	cycles with 0.5% total strain amplitude.	36
Fig. 20.	A new grain formed near a twin in Ni after 300 cycles	
	with 1% total strain amplitude.	37
Fig. 21.	A new grain formed in the interior of a grain at the end	
	of a twin after 510 cycles with 0.5% total strain	
	amplitude.	37
Fig. 22.	The microstructure of a Ni specimen after 510 cycles with	
	0.5% total amplitude. The whole cross sectional area	
	perpendicular to the loading direction is revealed.	38
Fig. 23.	The microstructure in Ni after 300 cycles with 1% total	
	strain amplitude.	40
Fig. 24.	The microstructure in Ni after 200 cycles with 1% total	
	strain amplitude followed by a tension test until	
	complete DRX occurred.	40
Fig. 25.	True stress-strain curves of Ni. Curve 1 and 2 represent	
	the first and the 200th cycles, and curve 3 is the initial	
	part of the hardening curve in a subsequent monotonic	
	tension test.	42
Fig. 26.	The dislocation structure inside a Ni grain after 300	
	cycles with 1% total strain amplitude.	44
Fig. 27.	The dislocation structure around a grain boundary after	
	300 cycles with 1% total strain amplitude.	44
Fig. 28.	The dislocation structure within a Ni grain after monotonic	3
	tension test to a strain ϵ = 0.15.	45
Fig. 29.	The dislocation structure in Al after 720 cycles with 0.5%	
	total strain amplitude.	45

		Figure Captions	Page
Fig.	30.	The dislocation structure in Ni around a grain boundary	
		after 510 cycles with 0.5% total strain amplitude.	46
Fig.	31.	The dislocation structure in Ni of a large area around	
		a grain boundary after 300 cycles with 1% total strain	
		amplitude.	48
Fig.	32.	Surface markings on a Cu single crystal after 420 cycles	
		with 1% total strain amplitude. (Due to the cylindrical	
		specimen shape only a small strip is in focus)	49
Fig.	33.	Qualitative decomposition of the cyclic flow stress.	52
Fig.	34.	DRX in Pb-2% Sn alloy after 50 fatigue cycles at a strain	
		amplitude of ± 0.75 % and frequency 5.5×10^{-3} Hz.	
		Recrystallization (a) at grain boundaries and (b) adjacent	
		to a high density of slip bands [39].	54

I INTRODUCTION

When a material is subjected to or even deformed at high temperatures, the microstructure and consequently the properties may change and cause failure. One well known high temperature phenomenon is the recrystallization of the material during deformation, also referred to as dynamic recrystallization (DRX). DRX has been reported in a variety of fcc metals and alloys in which the degree of dynamic recovery is restricted, such as Cu [1,2], CuAl [3], CuZn [4]; Ag [5]; Ni [6,7], Ni-Fe [7], Ni superalloys [8]; stainless steel [9], etc.. These experimental reports were based on the tests conducted in monotonic loading conditions, namely in tension, compression, or torsion. In a recent paper, DRX was found at the grain boundaries during low cycle fatigue (LCF) in bicrystals of Ni with special grain boundaries [10]. But no systematical research has been reported yet on DRX during LCF.

Most parts under high temperature service conditions, however, are subjected to cyclic loading conditions due to vibration or temperature fluctuations. A major difference between cyclic and monotonic loading is that the strain amplitude under cyclic conditions is commonly small compared to the critical strain to set off DRX in monotonic tests. However, the critical conditions for DRX to occur are determined by the microstructure, namely by the development of a cell-or subgrain structure[2,6,11]. In recent investigations on LiF [12], stainless steel [13,14,15] and Cu [16] it was found that also during LCF at elevated temperatures a microstructure develops that strongly resembles the dislocation structure, which occurs in high temperature monotonic

tests. Under appropriate conditions this microstructure may collapse and set off DRX.

Extensive grain boundary migration was observed during LCF. For monotonic tests at lower strain rates, the nucleation of DRX may occur by bulging of an existing grain boundary [7]. Also DRX caused by the bulging of original grain boundaries was reported on polycrystalline dilute Cu alloys [17]. Therefore, the grain boundary migration during LCF may set off DRX at a lower stress than the critical recrystallization stress for monotonic tests.

In the present study the problem was addressed by investigating the microstructural development during LCF.

II LITERATURE SURVEY

2.1 Grain Boundary Migration During LCF

It is clear from the data available to date that the movement of grain boundaries is an important microstructural process in high temperature fatigue. Quantitative studies have been reported on Pb [18,19] and Al [20,21]. Metallographic observations show that there is a one-to-one correspondence between the markings from grain boundary migration and the number and pattern of cyclic loading. Apparently, the grain boundaries respond to the imposed stresses by migrating in a cyclic manner and it is assumed that migration occurs such as to move the boundaries into a diamond shape grain configuration at 45° to the stress axis. The average distance of grain boundary migration \bar{m} for polycrystalline Al with strain amplitude less than $\approx \pm 0.48$ was found to obey the empirical relationship

$$\bar{m} = Af^{-0.35} \, {\stackrel{0.5}{N}} \, {\stackrel{0.66}{\Delta}} \, \exp(-62.0/RT)$$

where f : frequency

N : number of loading cycles

 $\Delta \epsilon$: strain amplitude

R : gas constant in kJ/mol.k

T : absolute temperature

A : $\approx 3.2 \times 10^{7} \mu ms^{0.35}$

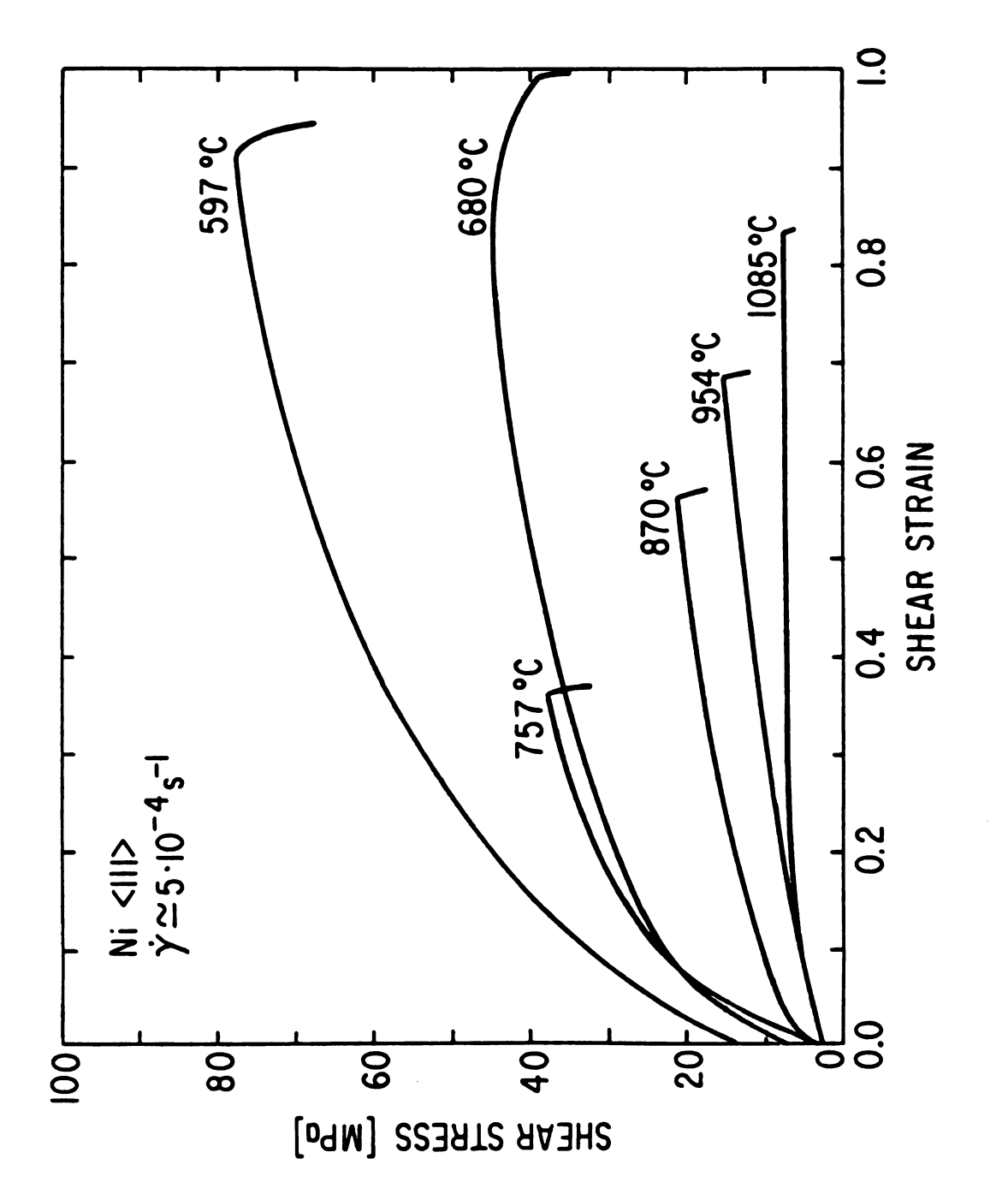
Also, the occurrence of cyclic migration leads to the disappearance of grains and thus is a mechanism of grain coarsening.

A change of the grain morphology due to grain boundary migration during cyclic deformation at 650° C at a low strain rate ($\dot{\epsilon}$ = $4\times10^{-4}/s$) was also reported on OFHC Cu [22]. But this change in grain shape was found to be strain rate dependent and at high strain rates, no such change in grain morphology occurred. That impurities or precipitates slow down or inhibit grain boundary migration explains why type 304 stainless steel does not exhibit any change in grain structure at 760° C at the lower strain rate.

A relation between grain boundary migration and nucleation of DRX was reported by Lim and Raj [10]. In their work on Ni bicrystals, they found that low to moderate extent of boundary migration was beneficial to the nucleation of fresh grains during LCF. They also found that grain boundary cavitation and migration were inversely related, i.e., in regions where migration had occurred there was little cavitation and vise versa.

2.2 DRX In Monotonic Tests

DRX has been investigated extensively in monotonic loading. As is known from previous investigations, the onset of DRX in single crystals is indicated by a sharp drop in the flow stress (Fig. 1) [5,23]. It has already been shown previously [24], the shear stress (τ_R) rather than shear strain (γ_R) is the critical quantity governing the initiation of



True resolved shear stress vs. true resolved shear strain for <111> Ni single crystal [6]. Fig. 1.

DRX. In single crystals, DRX is controlled by nucleation rather than by growth of recrystallized grains. In the same paper, they also showed that DRX is not only triggered but is also totally controlled by the deformation process. The growth of a nucleus is stopped by a strain rate increase, and, once stopped, it is not activated again in a subsequent recrystallization event. For a constant deformation path, i.e., same material, orientation, strain rate and temperature, DRX is set off reproducibly at a definite value of flow stress (r_{p}) . From the experiments on Cu and Ni Gottstein and Kocks [6] came up with a conclusion that dynamic recovery rather than a competing process, is a precondition to occurrence of DRX. Dynamic recovery of dislocations leads to rearrangement of cell walls on local scale giving rise to subboundaries [25] which being more mobile can form fluctuations in the homogeneous deformation structure and when subgrains of substantial area are formed can trigger DRX. Gottstein et al. [6] also found that two temperature regimes can be distincted with a rather sharp transition at $0.75 T_m$. The recrystallized structure was composed of discontinuously grown subgrains at very high temperature (vhT), or complete families of annealing twins at medium high temperature (mhT).

For nucleation mechanisms Karduck et al. [2] suggested

- (1) DRX is nucleated at vhT most likely by discontinous subgrain growth originating from kink bands owing to their special subgrain size and shape.
- (2) The nucleation of DRX at mhT is suggested to occur by emission of twins from subgrain boundaries. Twin formation is probably assisted by

internal stresses and favourable dislocation arrangements in the subboundaries.

For polycrystalline materials, as known, the grain boundaries influence the development of the dislocation structure as well as the recrystallization behavior. Hence, additional effects can occur in polycrystals so that the results on single crystals may not be sufficient to understand all recrystallization phenomena in polycrystalline aggregates. Sakai and Jonas [26] mentioned that there are two basic differences between single and polycrystal observations. The first is the initiation stress $(\tau_{\rm p},\sigma_{\rm p})$ in a typical single crystal oriented for multiple slip can be high as two or more times that in a polycrystal of the same conditions. The second difference is nucleation in polycrystals is large restricted to the original grain boundaries, in single crystals, it occurs in the grain interiors. They explained the difference of critical stress $(\tau_{\rm R},\sigma_{\rm R})$ was due to homogeneous nucleation for single crystals and heterogeneous nucleation for polycrystals. The initiation of DRX in polycrystals was also indicated by the drop of true stress as seen in Fig. 2 [27]. The strain rate has a strong influence on DRX. At the higher strain rates, the flow curve exhibits the typical shape for DRX, but at low strain rates, the flow curve is periodic due to recurrent cycles of recrystallization.

The mechanisms of dynamic nucleation have not been studied in as much detail as those of static recrystallization, it appears likely that grain boundary bulging as well as the mechanisms for single crystals are possible nucleation processes.

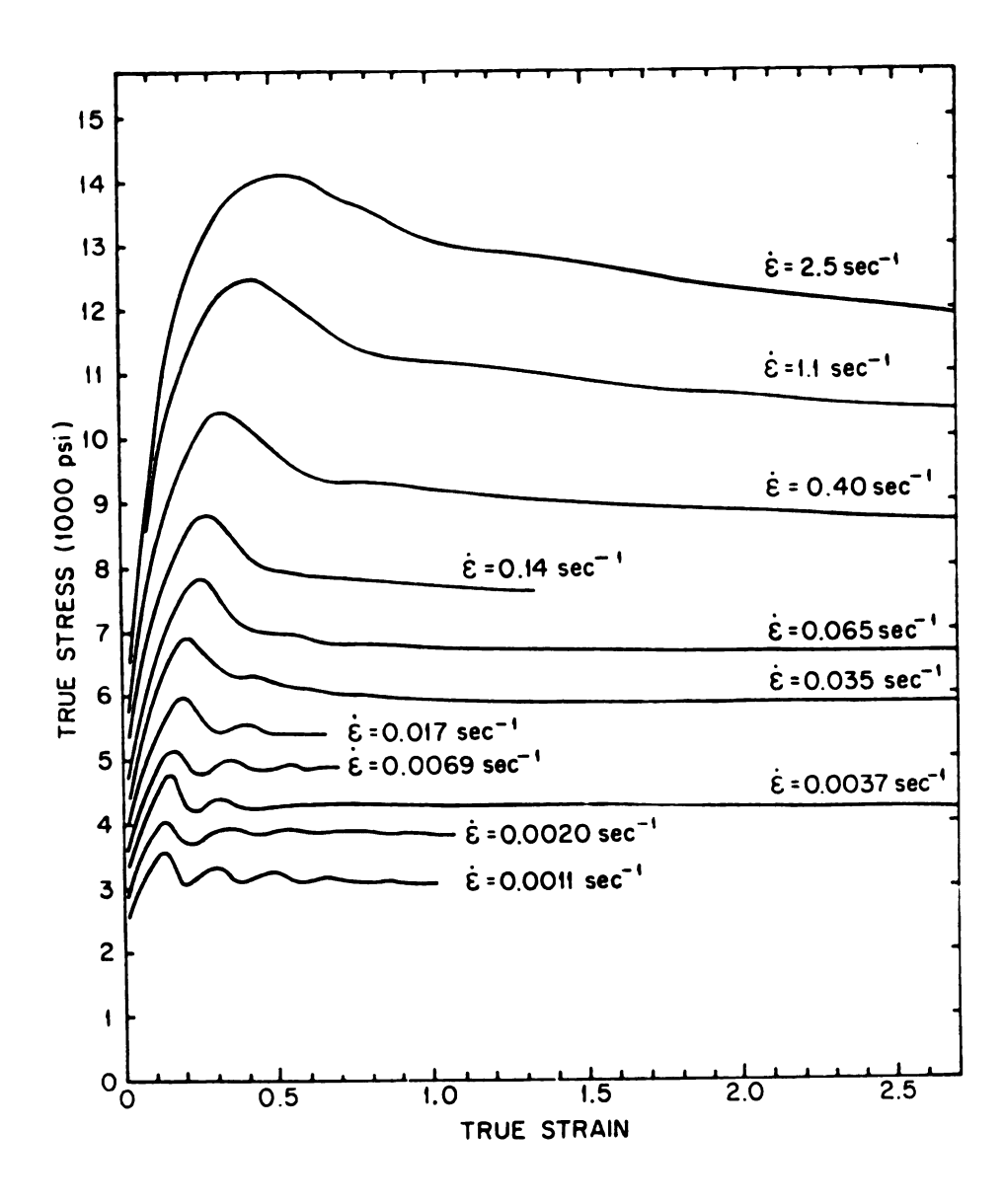


Fig. 2. Flow curves of a plain 0.25% C steel in the austenite state (fcc) at 1100° C (0.76 $T_{\rm m}$), illustrating the strong influence of strain rate [27].

2.3 DRX During LCF

The elevated temperature LCF effect on the mechanical behavior of structural material has attracted particular attention in recent years. Most investigations [28,29,30,31] focused on macroscopic parameters, though, such as stress, strain and cycles to failure, rather than on details of the microstructural evolution. Microstructural developments during LCF have been extensively studied during deformation at ambient temperature [32,33,34], but very few investigators have addressed the microstructural aspect of LCF at elevated temperatures. Recently, Moteff and collaborators [13,14 15] have studied the microstructural evolution of AISI 304 stainless steel at different fractions of the fatigue life. Their results show that at 0.5 T_m already in the first two cycles the dislocations tend to arrange in a cell structure which becomes progressively pronounced with increasing number of cycles, and finally will be converted to a subgrain structure with sharply defined boundaries. Majumdar and Burns [12] showed that LiF single crystals exhibit a fatigue behavior similar to that of fcc single/polycrystals and develop a celluar structure at high strain amplitudes and elevated temperatures. Konig and Blum [35] found in an investigation on Al that during RT creep in monotonic and cyclic loading the same steady state dislocation structure develops, so that the same deformation mechanism can be assumed for both types of test.

In a recent study on the nucleation of DRX in single crystals [6] it was found that DRX is triggered by dynamic recovery as a consequence of fluctuations in the recovery rate. This was attributed to the local appearance of mobile subboundary segments in an internally highly

stresses environment. The microstructural study of Nahm et al. [13] show exactly this arrangement of dislocations in fatigued specimens, so that critical conditions for DRX should also exist in cyclic deformation mode, although stress and instantaneous strain level remain comparably small in cyclic loading.

III EXPERIMENTAL PROCEDURE

3.1 Testing Materials

Very pure Ni polycrystals having the nominal compositions given in Table 1 were used. Also one Cu single crystal (99.999% pure) and two Al polycrystals with the composition given in Table 2 were tested.

Table 1 Composition of Ni studied

Element	:	Ag	A1	Cu	Fe <10	K	Li	Mg	Mo	Na	Pb
Wt ppm	:	<10	<10	<10		<10	<10	<10	<10	<10	<10
Element Wt ppm										Ni Bal.	

^{*} no information was given by the vendor (MRC). The concentration may be higher than 10 ppm but less than 130 ppm as typical in commercial Ni (grade 270).

Table 2 Composition of Al studied

Element Wt ppm	:	Ca . 22	Cu . 25	Fe .32	K . 22	Mg 3.5	Na <1.0	Si 1.4	Ce . 29
Element	:	C	C1	Н	N	0	P	Al	
Wt ppm	:	15	1.1	<1.0	<1.0	<5.0	. 29	Bal.	

3.2 Specimen Preparation

3.2.1 Mechanical Testing Specimens

(1) Ni polycrystal specimens were machined from 3/8" diameter rods. The specimen shape and dimensions are shown in Fig. 3. Two kinds of gauge length were chosen to avoid buckling when the test went to high strain amplitudes.

- (2) A Cu single crystal specimen was machined down the center section, using an electric discharge machine. This method confines the introduced cold work to a thin surface layer which can be removed chemically. The orientation of the stress axis was determined by the back-reflection Laue method. Specimen shape and orientation are shown in Figs. 3 and 4.
- (3) Al polycrystal specimens were machined from 3/8" diameter rods to the same shape as described for Ni.(see Fig. 3)
- (4) All specimens were annealed in a vacuum furnace at a pressure of approximately 10^{-5} Torr. The Ni specimens were chemically polished in the following solution at 70° C for 30 s to remove any surface irregularities,

glacial acetic acid 64 ml
nitric acid 34 ml
hydrofluoric acid 1 ml

and then were annealed at 800° C for 5 hours. The Al specimen was annealed at 310° C for 5 hours. The Cu single crystal specimen was chemically polished to remove 0.1 mm from the surface to avoid any potential sites for recrystallization during annealing, using the following solution

phosphoric acid 33 ml glacial acetic acid 33 ml nitric acid 33 ml

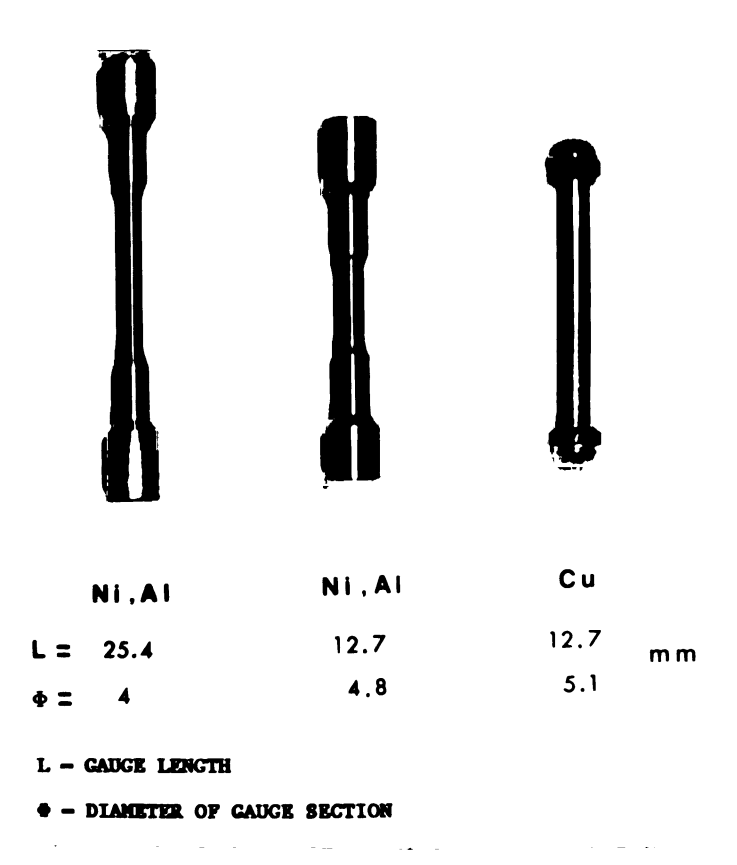


Fig. 3. Geometry and dimensions of testing samples.

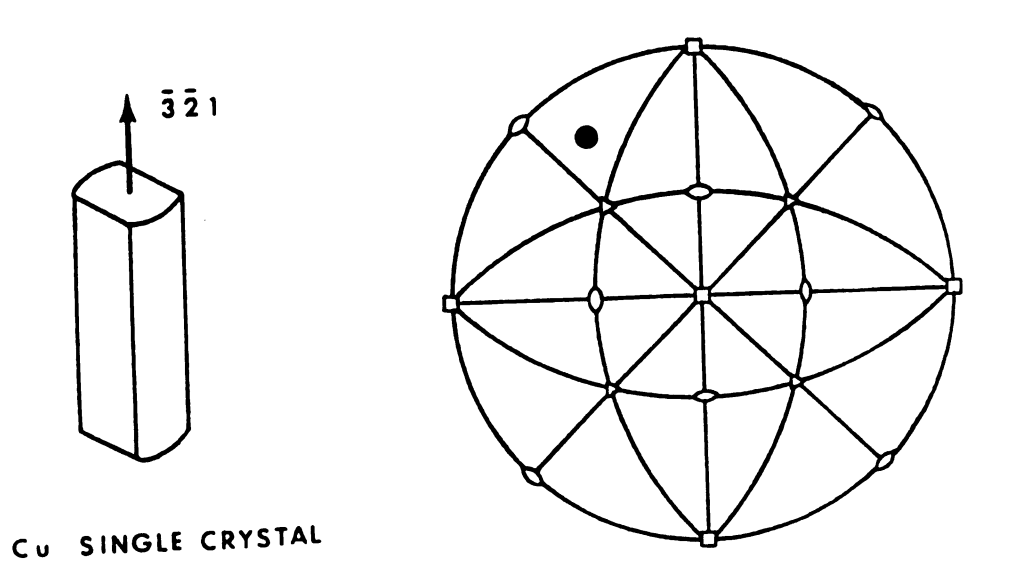


Fig. 4. Gauge sectional geometry and orientation of the Cu single crystal.

Subsequently, it was annealed at 800 °C for 12 hours.

3.2.2 Optical Microscopy Specimens

Some of the optical micrographs were taken directly from the planar side surface of the specimen when the test was interrupted after some cycles. The others were taken after the end of the tests. Specimens were cut from test samples with a very slow speed diamond wheel cutting machine along a plane perpendicular to the stress axis. Subsequently they were mounted in cold setting resin before mechanical polishing. All specimens were first polished on abrasive grit paper and then on a cloth by using aluminum oxide to get a mirror-like surface.

The etchants were

nitric acid		67	ml			
glacial acetic acid		33	ml			
hydrochloric acid		1	ml	for	Ni	
hydrofluoric acid		46.2	ml			
water		46.2	ml			
hydrochloric acid		7.6	ml	for	Al,	and
ammonium hydroxide	≈ 58%	50	m1			
water		50	ml			
hydrogen peroxide	≈ 30%	25	m1	for	Cu.	

All optical micrographs were taken with a Neophot 21 Microscope.

3.2.3 Electron Microscopy Specimens

Slices of approximately 0.3-0.4 mm thickness were sectioned from testing samples, using an Isomet low speed saw with diamond wheel such that the foil plane normal is parallel to the direction of loading. These slices were thinned down to 0.1 mm by careful mechanical polishing.

The final jet polishing was done in a Tenupol jet polishing device. Electrolytes used were A8(*) for Ni and A7(*) for Al. The optimal jet polishing conditions are given in Table 3.

Table 3 Jet polishing conditions for Ni and Al

	Electrolyte		Temp (°C)	Voltage (V)	Current (A)
Ni	A8 acetic acid perchloric acid	950 ml 50 ml	13	70	0.18
Al	0	100 ml 200 ml 700 ml	-510	12	0.12

^{*} A7 and A8 are registered trade marks of Struers Scientific Instruments, Inc..

All specimens were examined in a Hitachi H-800 electron microscope with double tilt specimen holder. The applied voltage was 200 kV.

3.3 Mechanical Testing

All tests were conducted on a floor model electro-mechanical Instron testing machine with a 500 kg tension-compression reversible load cell.

Pull rods and button head grips were designed and machined out of

310 heat resistant stainless steel.

To avoid oxidation of the specimen during testing a cylindrical protective chamber was designed as shown in Fig. 5. A stainless steel ring with a clearance of 0.75 mm to the pull rod was welded at the top of the tube, while the lower ring which fitted on the lower pull rod was made of Invar and the dimensions were chosen such that at temperatures in excess of 200 °C a tight fit with the lower pull rod was obtained due to the difference in thermal expansion between Invar ring and lower pull rod.

With this chamber design a protective atmosphere of 90% $N_2 + 10\%$ H_2 was maintained during the test inside the chamber to minimize oxidation. A flow rate of 12 liters/hour at 5 psi of this gas mixture was found sufficient to avoid oxidation. Higher flow rates were avoided since the gas started burning at the top of the chamber, also it created an unwanted back pressure.

Computer codes were developed in house to control the Instron testing machine by the digital output from an IBM XT personal computer and for data aquisition by A/D conversion of the load cell signal. This enabled to store all the load-displacement data from the test at an interval chosen properly. The resolution of data aquisition was 4 μ m per data set with an accuracy better than 0.1%. This data was then further processed to get the relevant information such as true stress-strain curves and work hardening coefficient vs. true stress curves, etc..

All tests were conducted with an initial strain rate of approximately 2×10^{-4} s⁻¹. The cycle frequency depended on strain amplitude range from 2×10^{-2} Hz to 7×10^{-3} Hz, corresponding to a total strain amplitude of 0.375% to 1%, respectively.

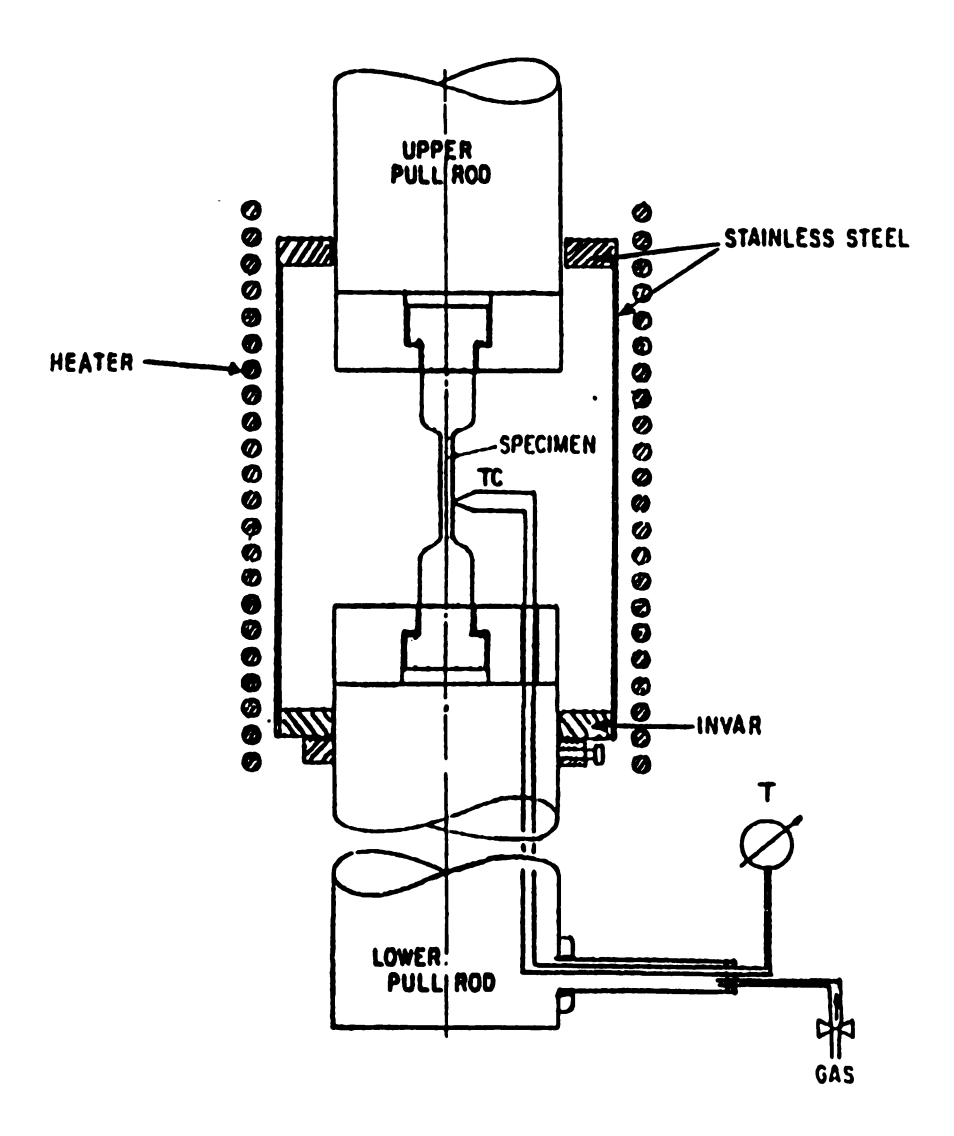


Fig. 5. Arrangement of the high temperature mechanical testing setup.

The test temperature was selected to approximately half the melting temperature, that is, 600° C for Ni, 200° C for Al and 400° C for Cu. The test temperature was kept constant within $\pm 2^{\circ}$ C.

3.4 The Microhardness Test

The microhardness was adopted to measure the hardness distribution of the microstructure. The diamond-pyramid hardness number (DPH), or Vickers hardness number (VHN, or VPH) was determined from the following equation [36]

DPH =
$$\frac{2P\sin(\theta/2)}{L^2} = \frac{1.854P}{L^2}$$

where P - applied load, kg

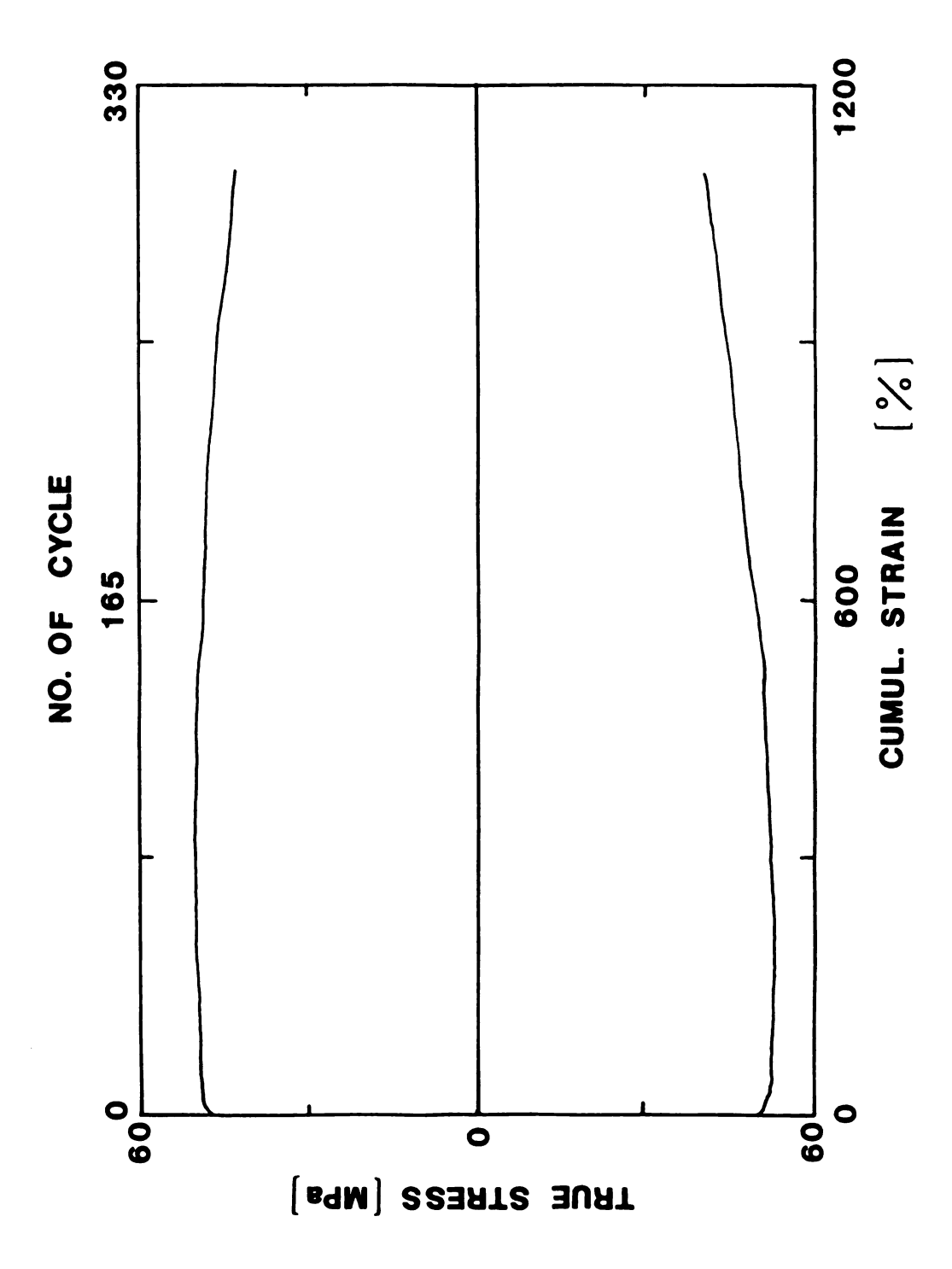
L - average length of diagonal, mm

 θ - angle between opposite faces of diamond - 136 $^{\circ}$. The applied load in the test was 0.1 kg.

IV EXPERIMENTAL RESULTS

4.1 Mechanical Behavior

In cyclic deformation the total strain amplitude was kept constant for each test. One testing result was shown in Fig. 6. This curve was plotted in terms of the stress amplitude as function of the cumulative strain. The total strain amplitude (elastic + plastic) for this test is 1%. In the first several cycles the true stress increases rapidly due to the initial high strain hardening and then reaches saturation. After about 100 cycles deformation the stress continuously decreases. The stress decrease indicates a strong softening mechanism to occur at large cumulative strains. Fig. 7 and Fig. 8 are the testing results corresponding to 0.5% and 0.375% total strain amplitudes respectively. Both show a maximum of the true stress after a large number of cycles, and then the stress decreases continuously. By decreasing the strain amplitude, the maximum point was shifted to a higher number of cycles, also the maximum stress became smaller. Fig. 9 is the testing result of Al with a 0.5% strain amplitude. The stress shows the same phenomenon as Fig. 6, but the rate of stress decrease $((d\sigma/\sigma)/dN)$ is smaller than that shown in Ni. Fig. 10 is the testing result of a Cu single crystal. The strain amplitude is 1%. It also exhibits a maximum stress and then decreases continuously.



True stress amplitude vs. cumulative strain of Ni with 1% total strain amplitude. Fig. 6.

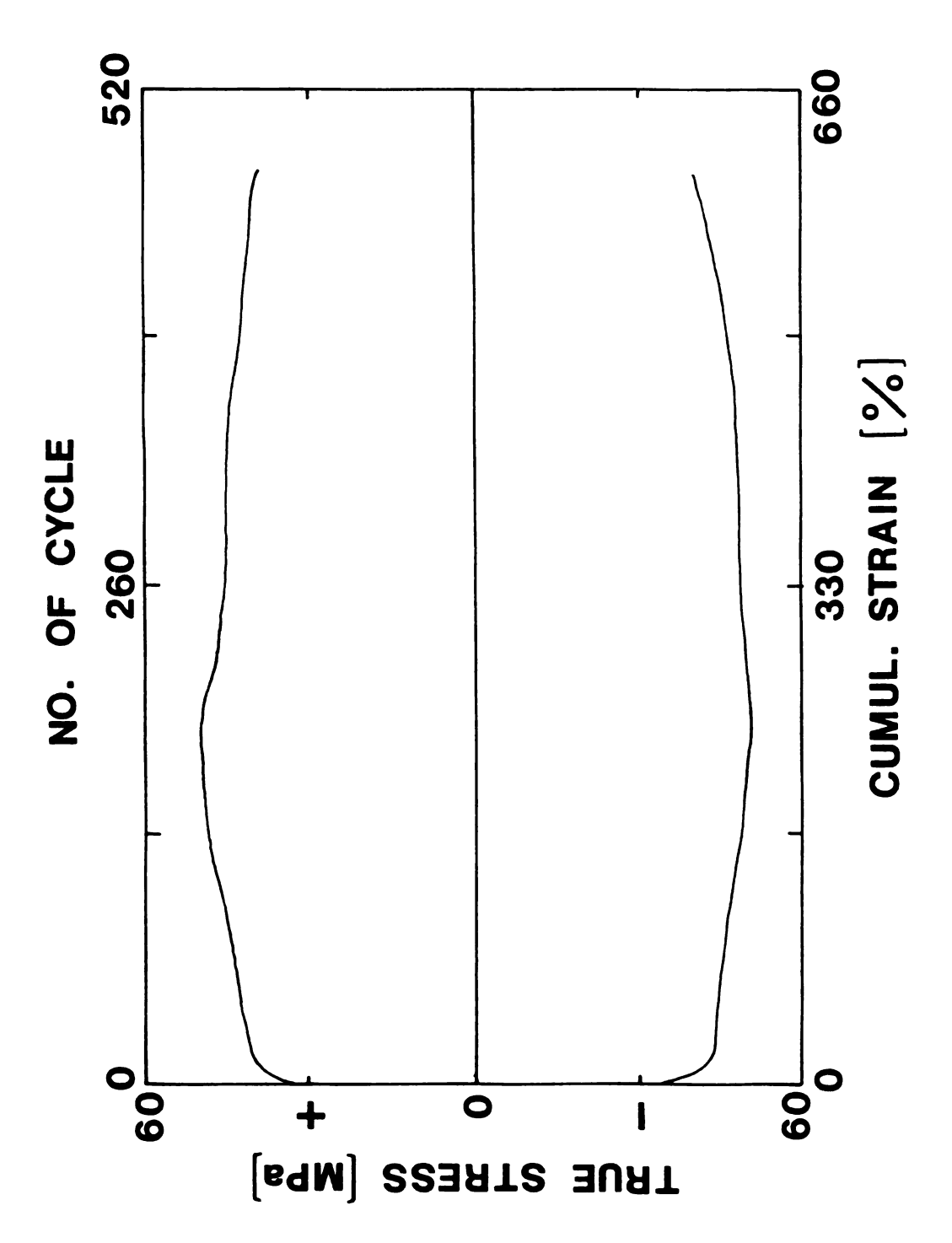
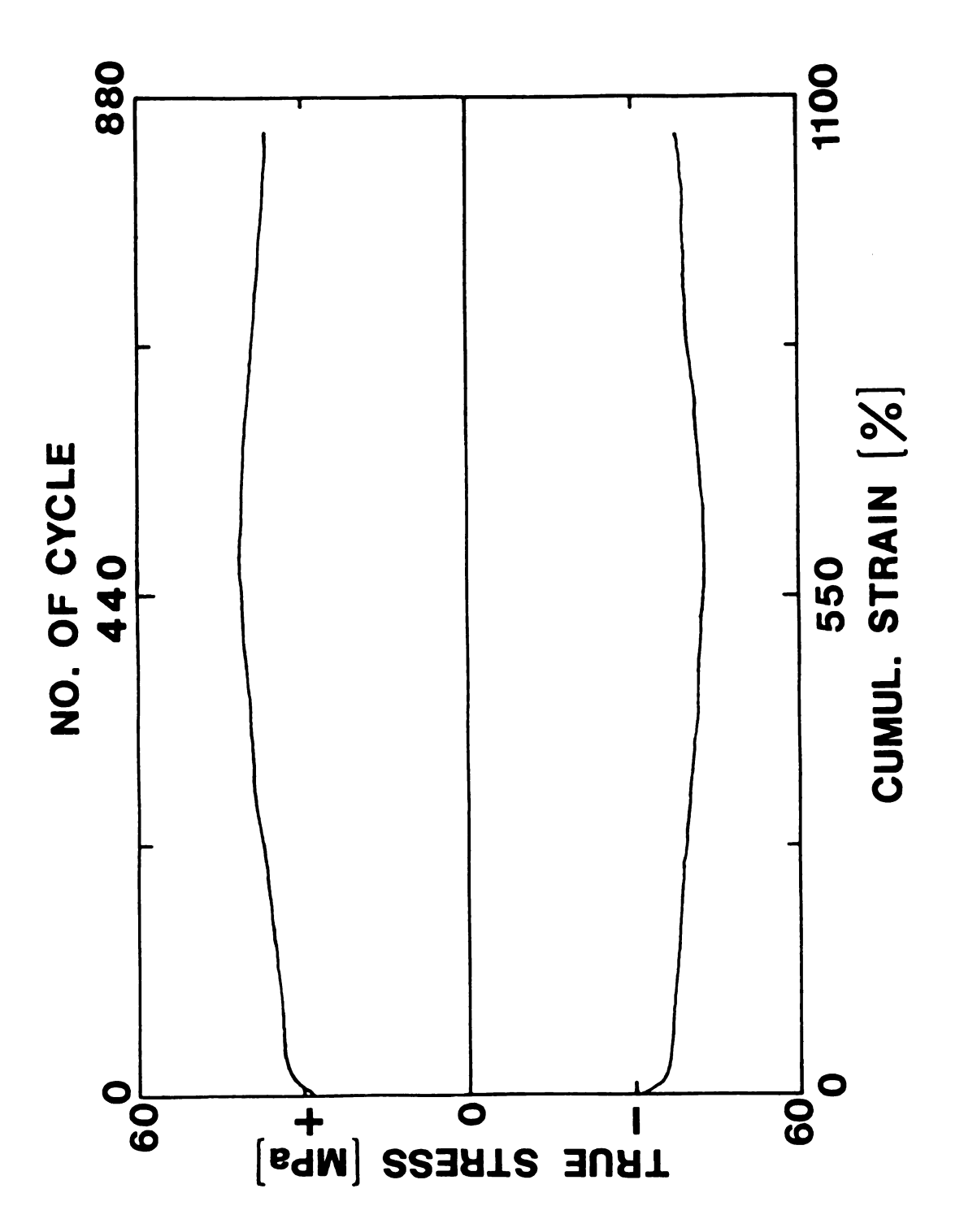
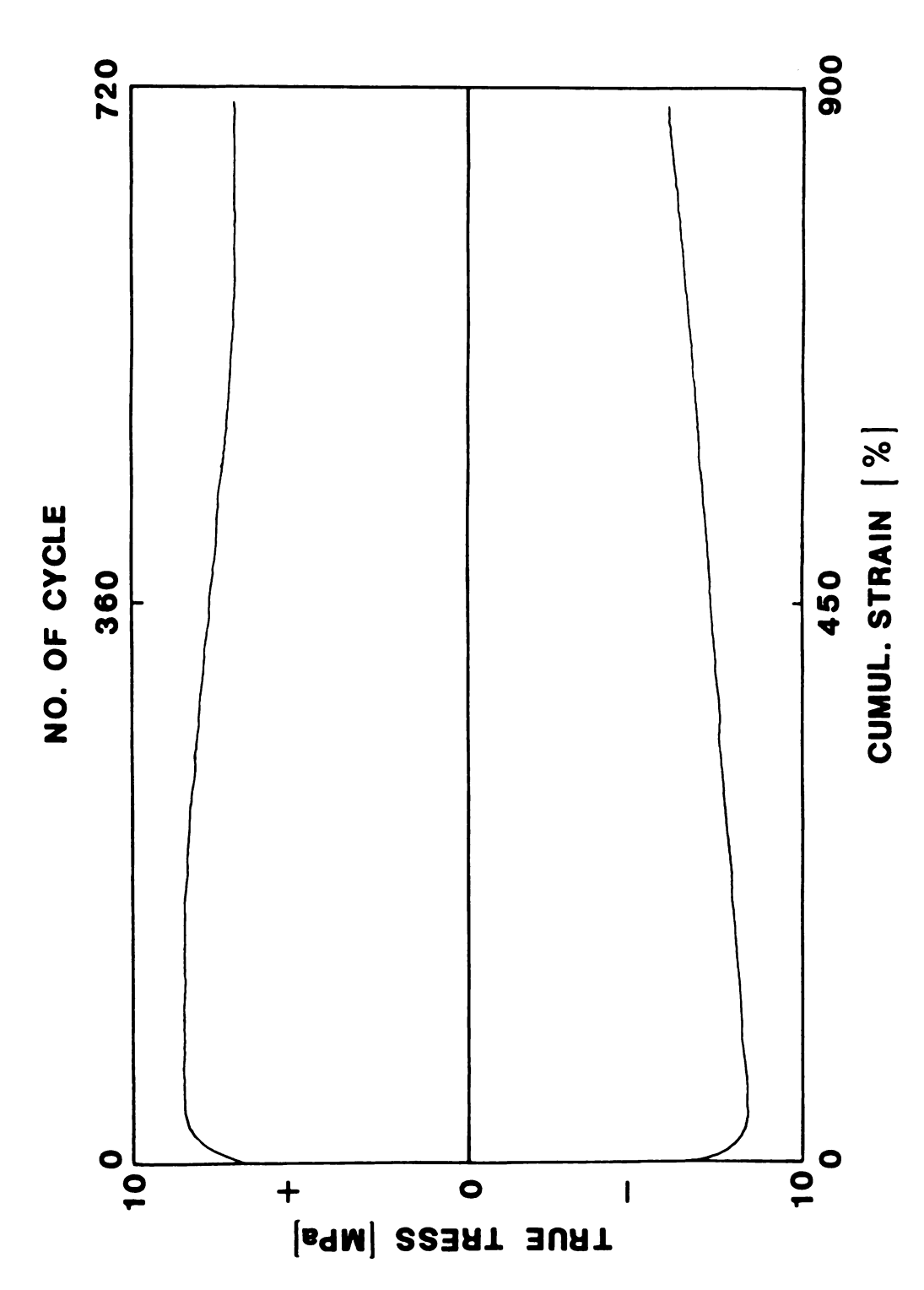


Fig. 7. True stress amplitude vs. cumulative strain of Ni with 0.5% total strain amplitude.



True stress amplitude vs. cumulative strain of Ni with 0.375% total strain amplitude. Fig. 8.



True stress amplitude vs. cumulative strain of Al with 0.5\$ total strain amplitude. Fig. 9.

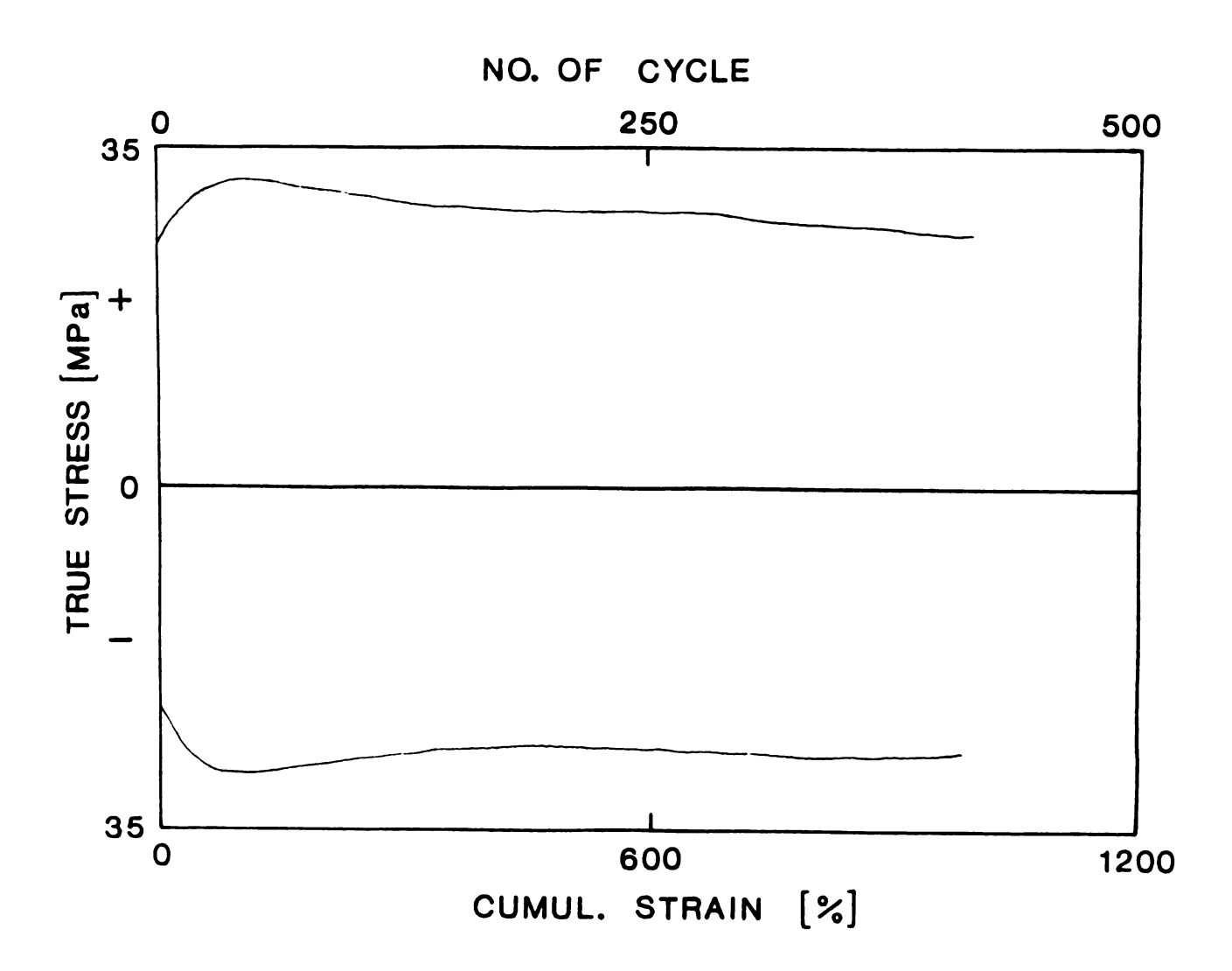


Fig. 10. True stress amplitude vs. cumulative strain of a Cu single crystal with 1% total strain amplitude.

4.2 Microstructural Development

Substantial microstructural changes were found when comparing the microstructures before (Fig. 11) and after the test (Fig. 12). changes are due to extensive grain boundary migration. In Fig. 11 most grain boundaries showed smooth curves, nevertheless, serrated segments and sharp turns were found in Fig. 12, which is the microstructure after 200 cycles deformation with 0.5% strain amplitude. In order to investigate the phenomenon more systematically, one specimen was machined flat on one side surface such that the microstructures could be examined after different deformation stages. The test was interrupted after 10 complete cycles, 40 cycles, and finally 160 cycles. A series of micrographs was taken after each specific stage. They are shown in Figs. 13 (a)-(j). All these micrographs were taken from the same area which was parallel to the loading direction. Fig. 13(a) is the microstructure of the annealed state. The average grain size as measured by the linear intercept method is about 300 μ m. There are many small grains embedded between large ones in this annealed state. Fig. 13(b) is the microstructure after 10 complete cycles. Position A, B and D show extensive grain boundary migration. One grain boundary disappeared and one twin boundary formed at position C. About 25 μm thickness was polished away in the sequence from Fig. 13(a) to Fig. 13(b). Comparing these two microstructures, it was found the small grains tend to shrink. Fig. 13(c) is the microstructure taken immediately after 10 cycles. The strain distribution is inhomogeneous in that some areas show much stronger grain boundary migration. The grain boundary arrangement is complex because of the superposition of grain boundary positions of all previous cycles due to grain boundary

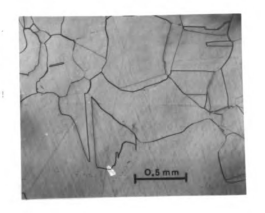




Fig. 11. The microstructure of Ni after annealing at 800 $^{\rm O}$ C for 5 hours.

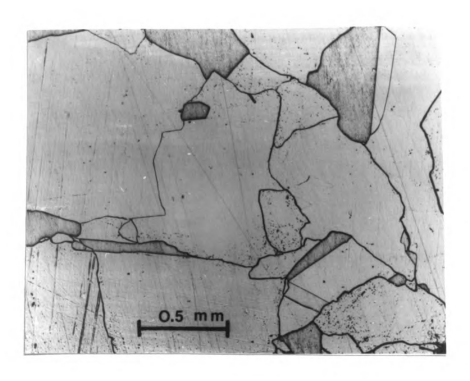
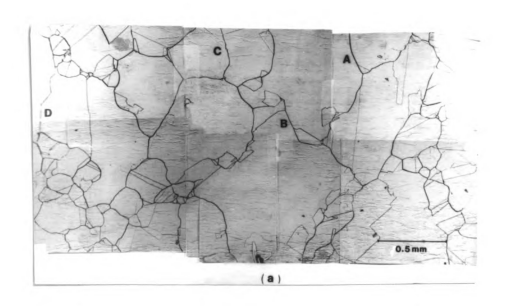


Fig. 12. The microstructure of Ni after 200 cycles with 0.5% total strain amplitude at $600\,^{\circ}$ C.

sliding perpendicular to the surface. Therefore, the sample was etched again slightly such that the boundary position before and after deformation could be seen simultaneously. Fig. 13(d) is the result after etching. The grain boundary at position B in Fig. 13(c) reveals a series of approximately parallel markings in front of this grain boundary. The new grain boundary position can be seen in Fig. 13(d). Those markings delineated the positions of the boundaries at the end of each stress cycles. A one-to-one correspondence between the number of grain boundary markings and the total number of whole cycles imposed on the specimen was established. A more detailed structure of surface markings is shown in Fig. 14. The same procedure was followed for the investigation at higher numbers of cycles. Figs. 13(e)-(g) are the microstructures after 40 cycles. They show the same phenomenon, but the migration rate has decreased compared to the first 10 cycles. positions indicated by arrows make it is obvious that the grain boundaries tend to migrate such as to align under 45 with respect to the stress axis. This will facilitate the grain boundary sliding and is believed to also may cause cavity formation. Figs. 13(h)-(j) are the micrographs after 160 cycles. Although compared to Figs. 13(e)-(g) the sample had deformed another 120 cycles, Fig. 13(j) doesn't show much difference compared to the microstructure in Fig. 13(g), except most grain boundaries now are aligned under 45 to the stress axis. average grain size of the sample after 160 cycles (Fig.13(j)) approximately 400 μm .

Grain boundary migration was also observed in Al. The micrographs in Fig. 15(b) were taken after 720 cycles deformation. Actually, it is the whole cross sectional area perpendicular to the loading direction.



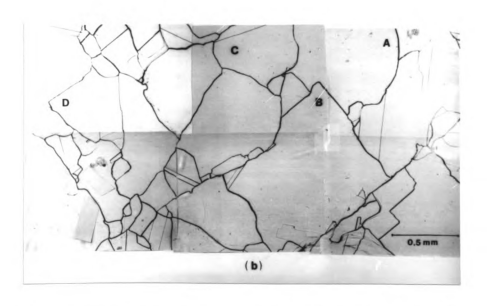
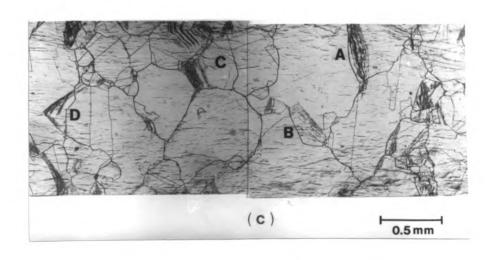


Fig. 13. The microstructures of Ni in a plane parallel to the loading direction after cyclic deformation with 0.5% strain amplitude at 600° C (a) Annealed at 800° C for 5 hours; (b) after 10 complete cycles at 600° C, slightly polished and etched again to reveal the new grain boundary positions;



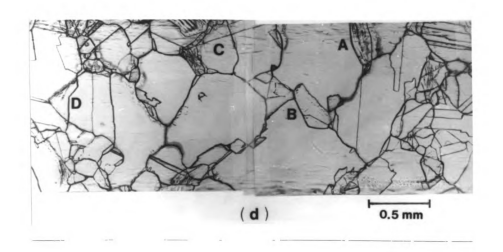


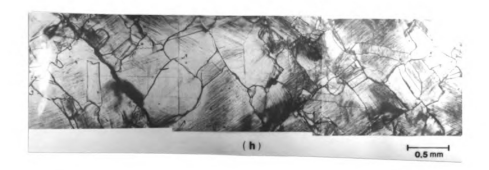
Fig. 13. (c) right after 10 complete cycles, positions A, B,C and D indicate inhomogeneous strain distribution on the surface; (d) etched to reveal the positions of new and original grain boundaries simultaneously;

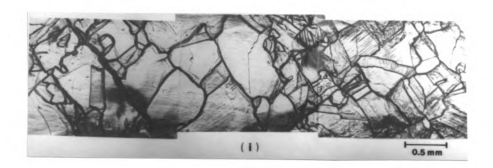






Fig. 13. (e) right after 40 cycles; (f) the positions of new and original grain boundaries after etching again; (g) slightly polished and etched again, only new grain boundaries can be seen;





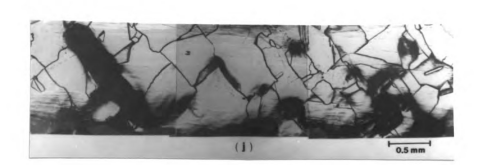


Fig. 13. (h) right after 160 cycles; (i) after etching; (j) after polishing and etching.

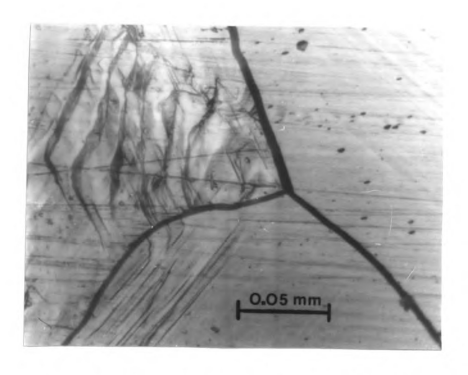


Fig. 14. Detailed structure of a surface marking after 10 cycles.

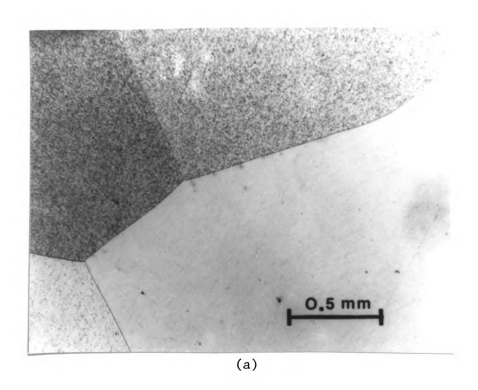


Fig. 15. The microstructure of Al (a) after annealing at $310^{\circ} \mathrm{C}$ for 5 hours;

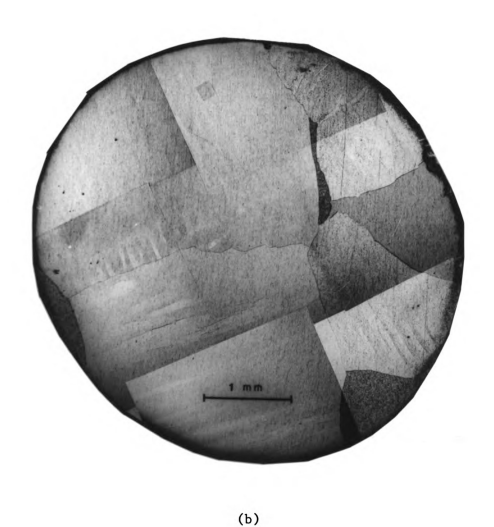


Fig. 15. (b) after 720 cycles with 0.5% total strain amplitude at 200 $^{\circ}\text{C}$. The two figures are not taken from the same area.

The grain boundary migration can be seen by comparison of Figs. 15(a) and (b). Fig. 15(b) shows curved grain boundaries instead of perfectly straight ones shown in Fig. 15(a), which is the microstructure of undeformed specimen.

4.3 Evidence Of DRX Under LCF

The occurrence of DRX in polycrystals is difficult to evidence since the sample remains polycrystalline and the newly formed grains are rapidly deformed by the concurrent deformation. It is particularly difficult in LCF because of the small driving forces and thus small boundary migration rate. The occurrence of DRX was therefore indirectly confirmed by metallographic investigations. After each test, the sample was cut perpendicular to the loading direction, and examined the microstucture in details under higher magnification. Special attention was paid to observe the grain boundaries. Several micrographs are shown in Figs. 16-21. The grain boundaries show serrations (Fig. 16), sharp protrusions (Fig. 17) and even new grains (Figs. 17-21). phenomena are typical for the nucleation of recrystallization at grain boundaries [26,37]. Figs. 17,19-21 show the details near a twin. It occurs as if the twin was created during deformation. This is important, since recrystallization twinning was found to be the major nucleation mechanism of DRX in monotonic tests. This seems to indicate that these processes are nucleation phenomena of DRX. Fig. 22 is a micrograph of the whole cross sectional area perpendicular to the loading direction after 510 cycles with a total strain amplitude of 0.5%. The microstructure contains areas with many small grains. While

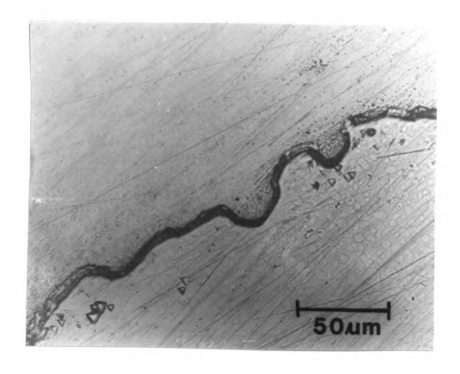


Fig. 16. Serrations of a grain boundary in Ni after 200 cycles with 0.5% total strain amplitude.

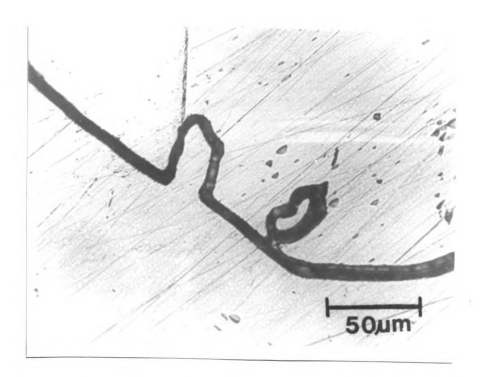


Fig. 17. A protrusion and a new grain at a grain boundary in Ni after 200 cycles with 0.5% total strain amplitude.

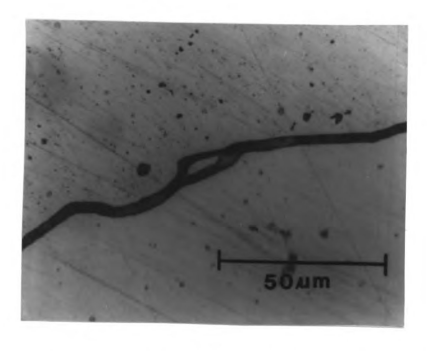


Fig. 18. A new grain on the grain boundary in Ni after 510 cycles with 0.5% total strain amplitude.

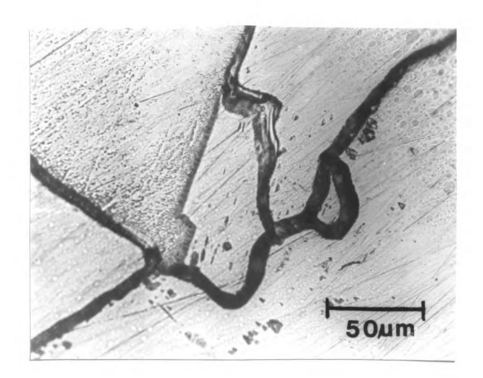


Fig. 19. A new grain formed at a twin boundary in Ni after 200 cycles with 0.5% total strain amplitude.

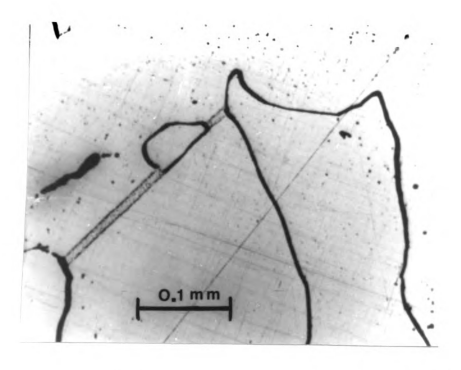


Fig. 20. A new grain formed near a twin in Ni after 300 cycles with 1% total strain amplitude.

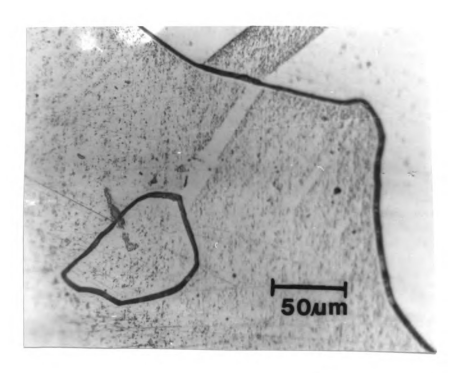


Fig. 21. A new grain formed in the interior of a grain at the end of a twin after 510 cycles with 0.5% total strain amplitude.

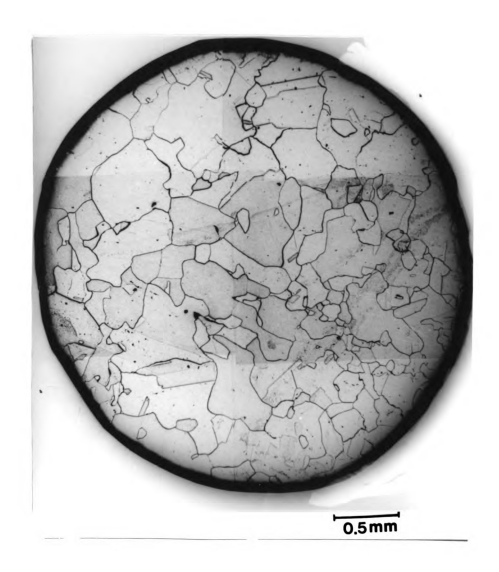


Fig. 22. The microstructure of a Ni specimen after 510 cycles with 0.5% total amplitude. The whole cross sectional area perpendicular to the loading direction is revealed.

the migration processes which were observed in the beginning of deformation, generally resulted in a coarsening of the microstructure, this micrograph, in contrast indicates a refinement of the microstructure. Fig. 23 shows the microstructure after 300 cycles with 1% strain amplitude. Compared to Fig. 22, the grain boundaries in this figure appear more snaky than in Fig. 22, also the nucleation phenomenon is more pronounced. Fig. 24 is the microstructure after 200 cycles cyclic deformation with 1% strain amplitude followed by a tension test until DRX occurred. This microstructure evidenced both boundary migration and DRX, but only DRX can be seen in monotonic tests.

A parallel study was conducted on Al. Due to the high stacking fault energy Al is not able to recrystallize during deformation [23,38]. Fig. 15(b) shows the microstructure of an Al polycrystal after 720 cycles deformation with a total strain amplitude of 0.5%. No small grains were detected in this micrograph. Obviously without DRX the microstructure has a tendency for uniform coarsening. The microstructure in Ni however shows local grain refinement. This further substantiates the conclusion that Ni polycrystals undergo DRX during LCF at high temperature.

Due to the lack of rapid quench equipment, the cooling rate of the sample in air was relatively slow. This might raise the problem that the microstructure after cooling to room temperature was not the same as the microstructure at high temperature before cooling. More to the critical point, the question is whether the observed recrystallization phenomena could be due to static recrystallization. This was tested by means of the flow stress which is very sensitive to recrystallization. A Ni sample was first cyclically deformed for 200 cycles with a total

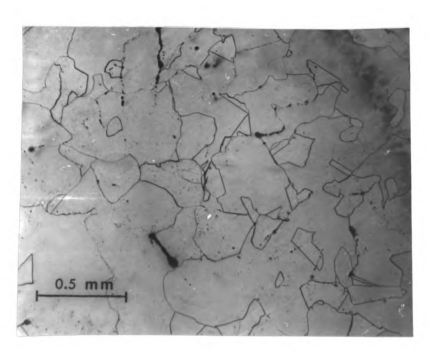


Fig. 23. The microstructure in Ni after 300 cycles with 1% total strain amplitude.

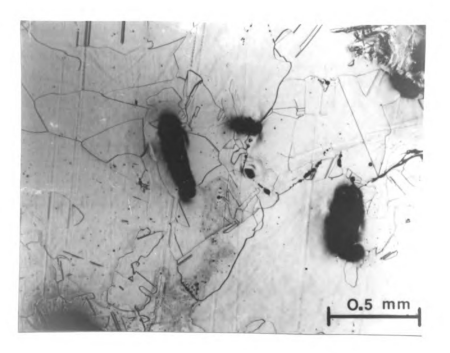


Fig. 24. The microstructure in Ni after 200 cycles with 1% total strain amplitude followed by a tension test until complete DRX occurred.

strain amplitude of 1% at 600°C and then kept under zero load at same temperature for 5 hours in the testing machine, and finally tested in tension until DRX occurred. The result is shown in Fig. 25. The true stress-strain curve of the first and the last (200th) cycles during cyclic deformation are indicated by 1 and 2 respectively in this plot. Curve 3 is the initial part of the hardening curve in subsequent monotonic tension test. The yield stress in curve 3 was measured as 40 MPa compared to 42 MPa which appeared in the last cycle under cyclic deformation. The small stress drop during annealing is typical for static recovery. This test substantiates that the recrystallization characteristics observed in the microstructure of fatigued specimens are not due to static recrystallization after the test but have to be attributed to DRX.

In addition microhardness tests were conducted to measure the hardness distribution of the grains shown in Fig. 22. The results are listed in Table 4.

Table 4 Hardness distribution in Fig. 22

Grain size [μm]	Average L [mm]	Average DPH
(a) >200	0.075 ± 0.001	33.0 ± 0.9
(b) <100	0.079 ± 0.001	29.7 ± 0.8

The average DPH of small grains is slightly but consistently smaller than that of large grains. This result is compatible with the

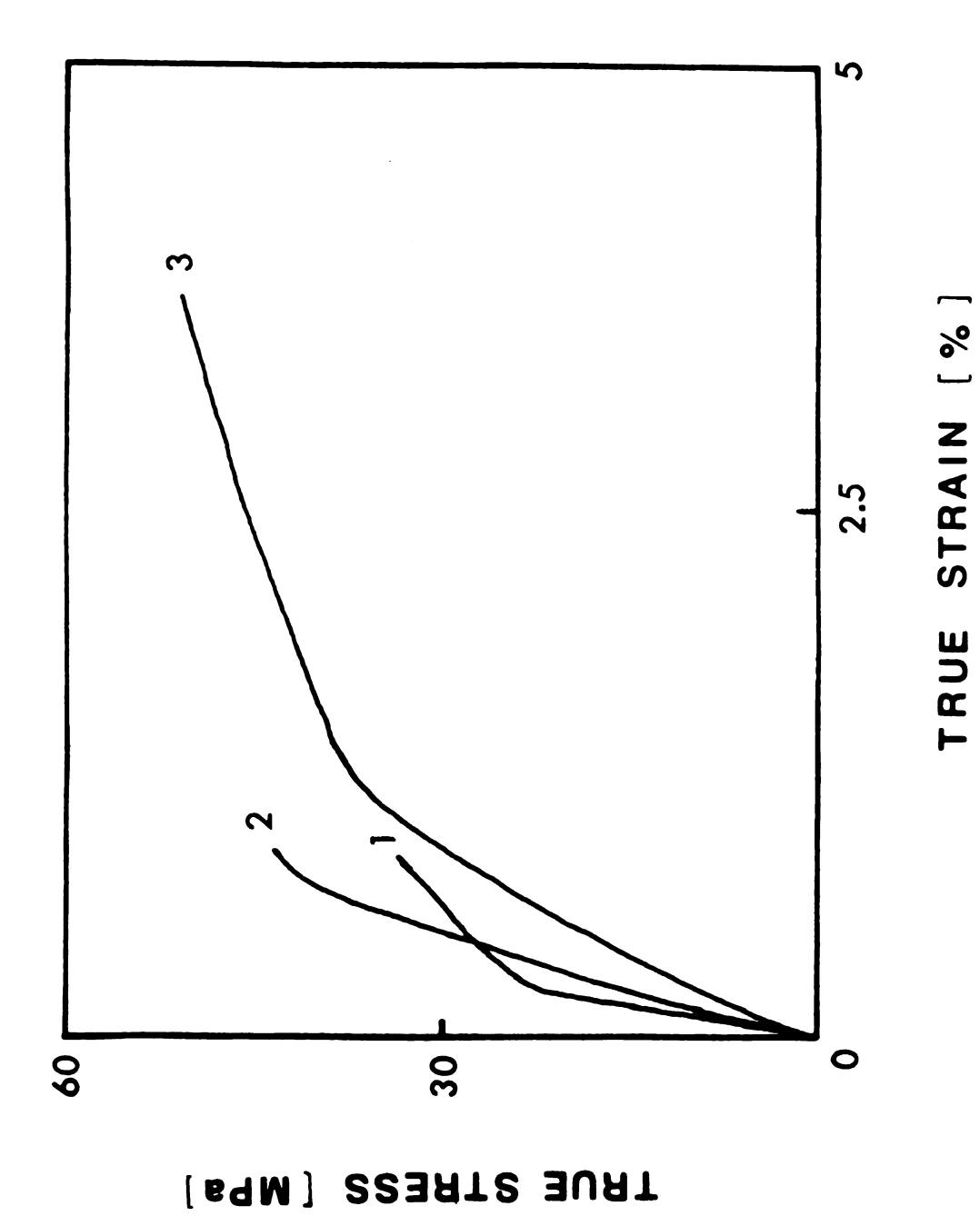


Fig. 25. True stress-strain curves of Ni. Curve 1 and 2 represent the first and the 200th cycles, and curve 3 is the initial part of the hardening curve in a subsequent monotonic tension test.

assumption that the small grains are nucleated by DRX. The relatively small difference in hardness can be attributed to the concurrent deformation which rapidly hardens the slowly growing recrystallized grains.

4.4 Dislocation Structures

Transmission electron microscopy was applied to examine the dislocation arrangement and development during LCF. Figs. 26 and 27 show the dislocation structure of Ni after 300 cycles with 1% strain amplitude. Both micrographs reveal a well developed cell structure inside a grain as well as close to a grain boundary. Compared to monotonic tests up to DRX at the same temperature and strain rate (Fig. 28) the structure of cyclic specimens appears more strongly recovered, and the cell size is considerably larger.

The dislocation structure of Al after 720 cycles was also examined (Fig. 29). The cell boundaries are less diffuse than in Ni (Figs. 27,30-31) under the same deformation conditions. The cell size is over 5 times larger than that of Ni, since the flow stress at the same strain amplitude is much smaller in Al than in Ni. This difference between Ni and Al reflects the impact of the higher specific stacking fault energy of Al and thus, a higher recovery rate.

Because of the observed extensive grain boundary migration, special efforts were made to observe the dislocation structure around grain boundaries. Fig. 30 shows the dislocation arrangement in a Ni

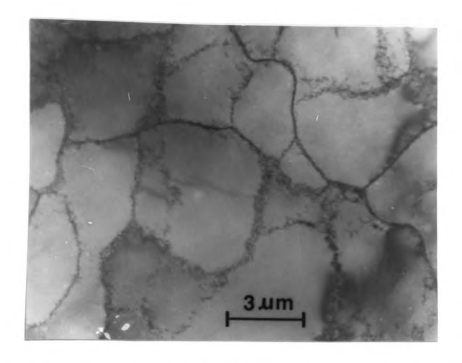


Fig. 26. The dislocation structure inside a Ni grain after 300 cycles with 1% total strain amplitude.

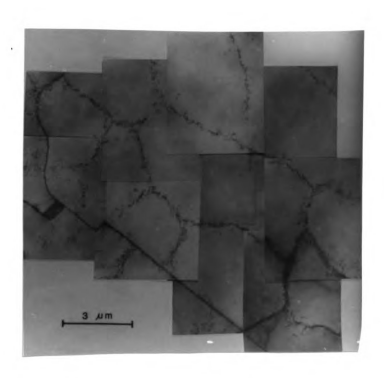


Fig. 27. The dislocation structure around a grain boundary after $300\ cycles$ with 1% total strain amplitude.



Fig. 28. The dislocation structure within a Ni grain after monotonic tension test to a strain ϵ = 0.15.

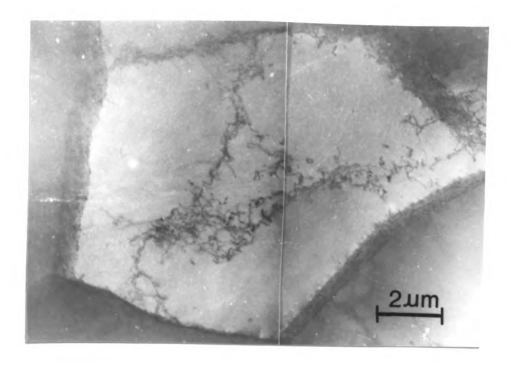


Fig. 29. The dislocation structure in Al after 720 cycles with 0.5% total strain amplitude.

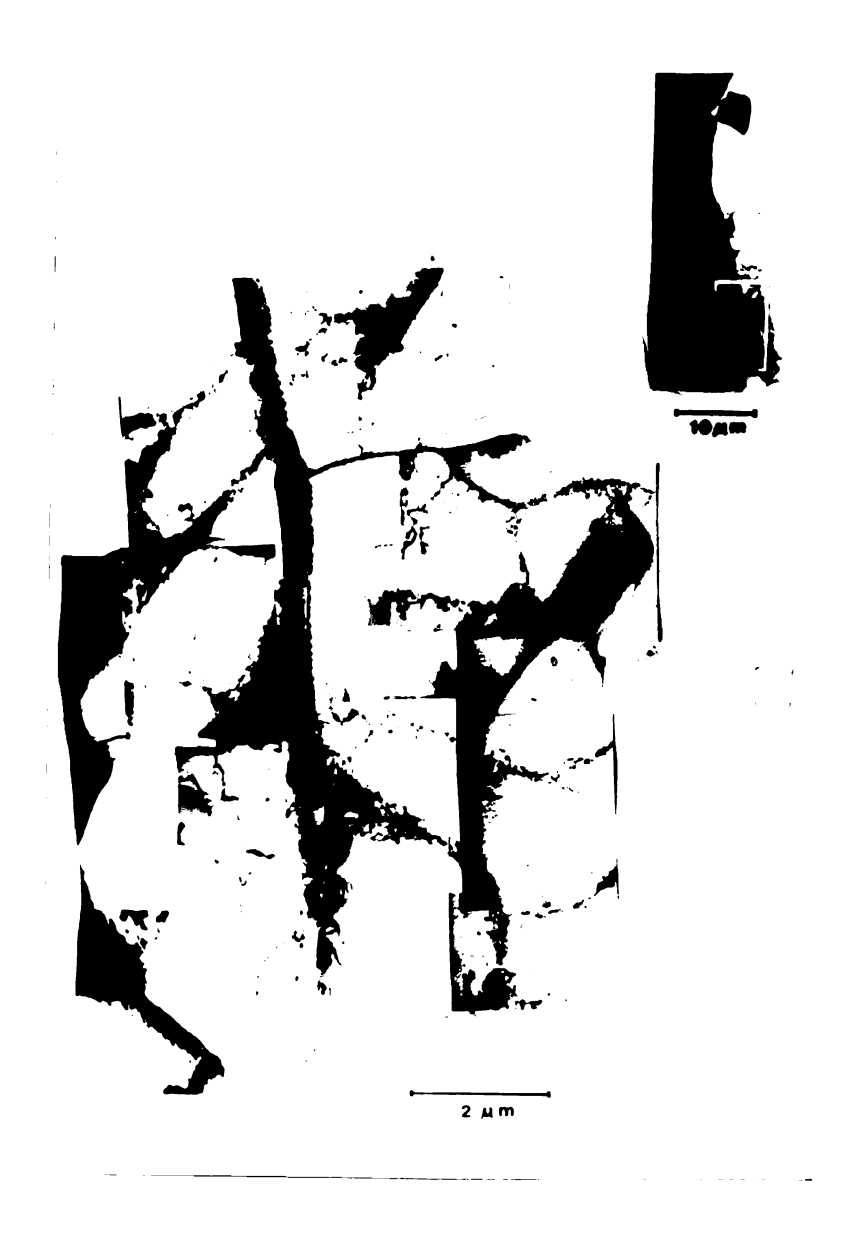


Fig. 30. The dislocation structure in Ni around a grain boundary after 510 cycles with 0.5% total strain amplitude.

polycrystal after 510 cycles with 0.5% strain amplitude. The right upper corner is the low magnification micrograph. It shows the curved shape of boundary. This curved shape suggests that the boundary migrated previously. In front of the grain boundary, dislocations form a distinct cell structure, but are not heavily tangled as in large strain monotonic tests (Fig. 28), rather they are loosely arranged in cell walls. Behind the boundary the cell interior is not so neat, and the cell walls are more diffuse. Such an arrangement is more typical for the beginning of cell formation and the arrangement indicates that it represents the new formation of a cell structure after the boundary swept the volume and eliminated the original structure. Similar phenomena were observed in a specimen deformed with 1% strain amplitude (Fig. 31). The grain boundary seems to migrate down to the right corner. Right behind the serrated boundary segment, the dislocation structure is ill recovered. In contrast, a well recovered cell structure is observed in front of or a little bit farther behind the serrated part of boundary. Despite the gradual difference it is surprising not to see a substantial difference in the dislocation density in front of and behind a moving boundary. It has to be taken into account however, that the microstructures reveal the dislocation arrangement after a large number of cycles where the grain boundary migration rate has slowed down essentially, while the concurrent deformation still reproduces dislocations.

4.5 Result Of A Cu Single Crystal

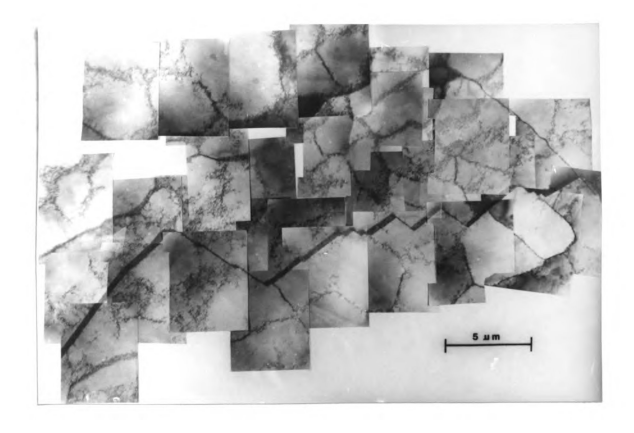


Fig. 31. The dislocation structure in Ni of a large area around a grain boundary after 300 cycles with 1% total strain amplitude.

In order to exempt the effect of grain boundaries during LCF, one Cu single crystal was tested under the same conditions of strain and temperature. Fig. 4 shows geometry and orientation of the sample. The orientation was such that [321] is parallel to the loading direction and deformation occurred by single slip. The strain amplitude was 1%. After 420 cycles the test was stopped and the specimen was examined under the optical microscope. Slip lines could clearly be seen on the surface (Fig. 32), but no recrystallized grains were detected. The sample was cut into many slices and carefully examined, but no indication of recrystallization was observed.

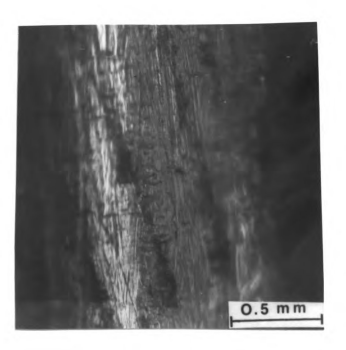


Fig. 32. Surface markings on a Cu single crystal after 420 cycles with 1% total strain amplitude. (Due to the cylindrical specimen shape only a small strip is in focus)

V DISCUSSIONS

Most grain boundaries in Ni and Al were found to show extensive migration during the test. Grain boundary migration phenomena were also reported on Pb [18,19] and Al [20,21] by Langdon et al.. They assumed that the boundary migration is stress-induced in response to the cyclic loading since the boundaries tend to align parallel to the plane of maximum shear stress. Since grain boundary migration will annihilate the dislocations in the swept volume, there ought to be a substantial differences in dislocation density in front of and behind a moving grain boundary. All TEM investigations failed to substantiate a drastic gradient in dislocation density across a boundary. Only qualitative difference in dislocation arrangements were noticed (Figs. 30-31). This does not mean though, that the grain boundaries do not absorb dislocations. Rather it has to be taken into account that

- (1) Grain boundary migration slows down at large number of cycles when the grain boundaries are essentially aligned 45 to the stress axis and all TEM investigations were conducted on specimens deformed to a large number of cycles.
- (2) DRX progresses very slowly because of a very small driving force.
- (3) The concurrent deformation constantly produces dislocations, and thus, replaces annihilated dislocations.

The investigated grain boundaries show strong evidence of interaction with dislocations by means of their high dislocation contents. This resembles the structure of slowly moving grain boundary observed after DRX in monotonic tests.

All cyclic hardening curves (Figs. 6-9) reveal a maximum followed by a continuous decrease of the true stress. The number of cycles to the flow stress maximum is the smaller the larger the cyclic strain amplitude. This behavior indicates a strong softening mechanism to occur at large cumulative strains. It is proposed to attribute this softening to grain boundary migration and DRX. DRX is known to occur in monotonic tests at relatively large strains and makes itself felt by a drastic decrease of the flow stress (Figs. 1-2). The softening observed in the current cyclic tests is much less spectacular because the net driving force for DRX in cyclic tests is much smaller than in monotonic The microstructural observations evidence extensive grain tests. boundary migration (Fig. 13) and the occurrence of new grains (Figs. 17-23) during LCF. Since grain boundaries are known to absorb dislocations during migration, this process will decrease the total dislocation density and thus, the flow stress. Qualitatively the hardening behavior can be understood by a superposition of strain hardening and softening due to grain boundary migration and grain growth (Fig. 33). At large strains the specimen continues to strain harden, but the strain hardening coefficient decreases owing to dynamic recovery, and DRX becomes increasingly stronger. This will finally lead to a maximum of the flow stress and a continuous stress decrease at larger strains.

Al also shows a hardening curve with a stress maximum, although the stress decrease rate $((d\sigma/\sigma)/dN \approx 3.2\times 10^{-4})$ is smaller than that of Ni $(\approx 5.9\times 10^{-4})$. (note also σ is considerably smaller for Al, under the same conditions). Al is known not to recrystallize dynamically due to its high stacking fault energy. In this case the stress has to be attributed totally to grain coarsening during cyclic deformation. This

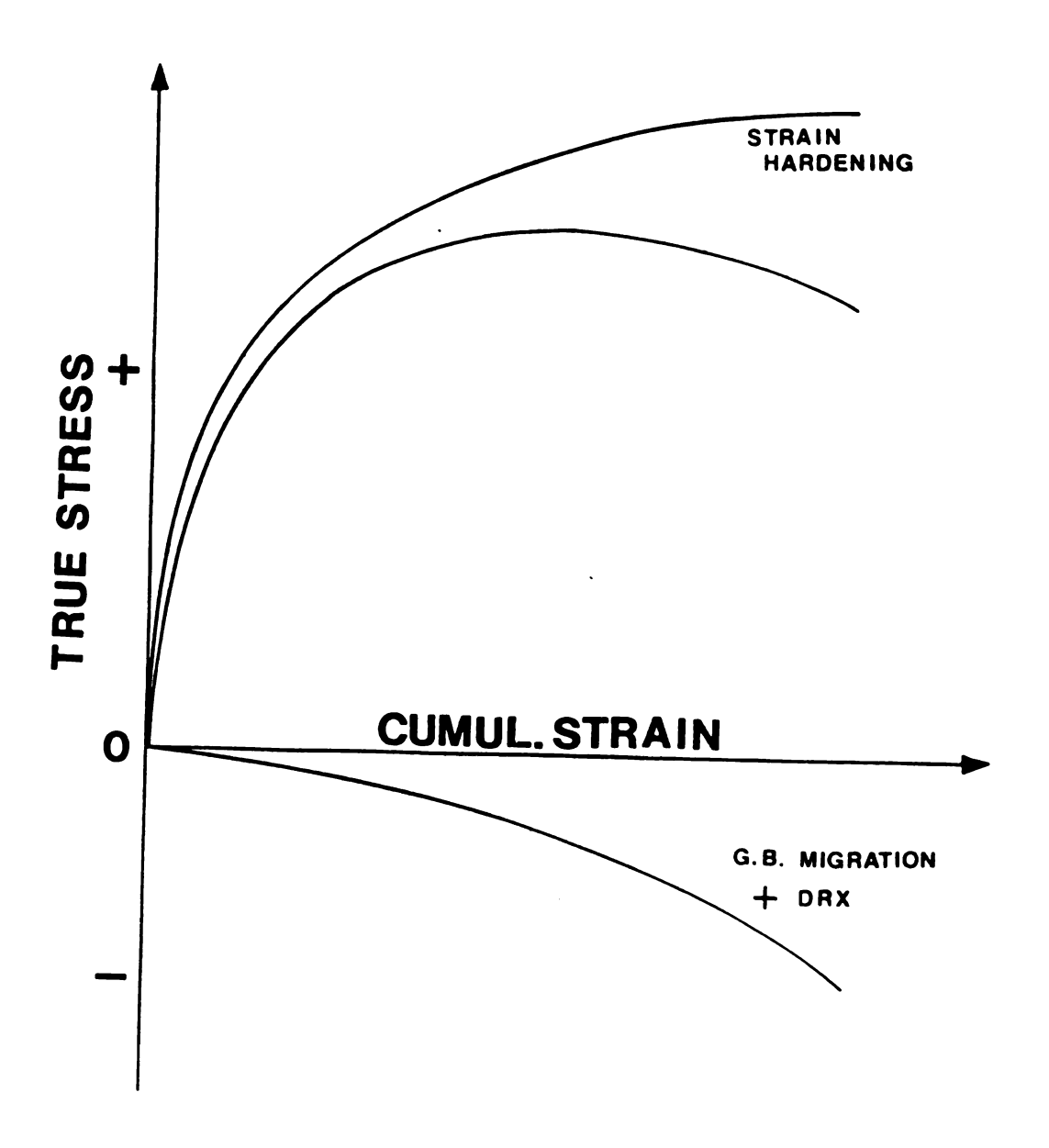


Fig. 33. Qualitative decomposition of the cyclic flow stress.

is also evident from the microstructure which reveals huge grains after cyclic deformation of Al. In contrast when the materials exhibits DRX, then the grain refinement due to DRX will reduce the softening effect caused by grain coarsening, but even in this situation Ni still shows a larger stress decrease rate. This substantiates that DRX is the major softening mechanism in Ni. DRX was also reported by Raman et al. [39] on Pb-2% Sn alloy. One micrograph from Ref. [39] is shown in Fig. 34. The new grains were observed at grain boundaries (Fig. 34(a)) and adjacent to a high density of slip bands (Fig. 34(b)). As is seen in Fig. 34(b), the newly formed grains also develop boundary markings due to the continuous cyclic deformation imposed on it. High temperature LCF on Ni-200 and dispersion strengthened (DS) Ni were investigated by Laird et al. [40,41]. But no DRX was reported in their works. This is probably due to the fact that the capacity for DRX also depends on the ease of migration of the grain boundaries, which decreases as the purity of the metal degrades [38]. Therefore, the existence of dispersed particles or impurities in the material that Laird and coworkers used, may totally suppress grain boundary migration and DRX. Also the cumulative strains in their works were small compared to present study and may be too small to set off DRX.

In monotonic tests, the onset of DRX can be associated with the drop of the flow stress. In cyclic tests this is doubtful, however, because the softening due to DRX is much smaller than in monotonic tests due to the low dislocation density, i.e., the low driving force. Also the concurrent deformation of the new grains will reduce the softening effect associated with these newly formed grains.

The investigated Cu single crystal did not show any DRX phenomenon in the current study. This indicates that grain boundary migration may play an important role for DRX during LCF, especially if the strain amplitude is low (\leq 1% in present investigation). A higher strain amplitude may activate DRX also in single crystals. It is not clear at this point why the cyclic hardening curve also shows a maximum despite the distinct absence of grain boundary migration and DRX. This has to be addressed in future research.

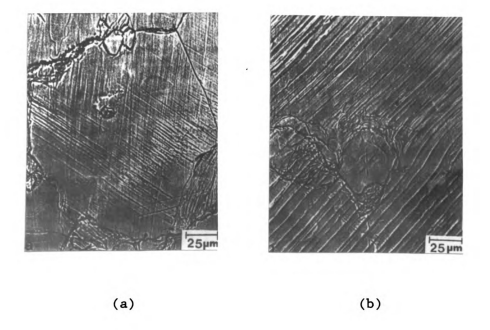


Fig. 34. DRX in Pb-2% Sn alloy after 50 fatigue cycles at a strain amplitude of ±0.75% and frequency 5.5×10⁻³ Hz. Recrystallization (a) at grain boundaries and (b) adjacent to a high density of slip bands [39].

VI CONCLUSIONS

The present investigations yield the following results:

- 1. Under cyclic deformation the flow stress amplitude as function of the cumulative strain shows a maximum after a large number of cycles, and then the stress decreases continuously. The cumulative strain at the maximum increases with decreasing strain amplitude. These results indicate a strong softening mechanism to occur at large cumulative strains.
- 2. Most grain boundaries show extensive migration. The migrating rate decreases as the number of cycles increases. The grain boundaries move such as to align under 45° with respect to the stress axis and thus maximize the grain boundary sliding.
- 3. Under cyclic deformation, even at a total strain amplitude as small as 0.375%, there is evidence that Ni also undergoes dynamic recrystallization. Dynamic recrystallization is likely to be the major softening mechanism during low cycle fatigue at high temperature. The microstructural investigations suggest that recrystallization twinning and grain boundary bulging may be responsible for the nucleation of dynamic recrystallization during low cycle fatigue.

4. Dynamic recrystallization was not observed during LCF of a Cu single crystal. This suggests that the grain boundaries play an important role in dynamic recrystallization during low cycle fatigue with small strain amplitude.

VII REFERENCES

- [1] G. Gottstein: Met. Sci., vol. 17, 1983, pp. 497-502
- [2] P. Karduck, G. Gottstein and H. Mecking: Acta Met., vol. 31, 1983, pp. 1525-1536.
- [3] R. Bromley and C.M. Sellars: The Microstructure and Design of Alloys (ICSMA 3), vol. 2, pp. 380-386, Institute of Metals, London, 1973.
- [4] B.J. Sunter and N.M. Burman : J. Australian Inst. Metals, vol. 17, 1972, pp. 91-100.
- [5] P.J.I. Stuitjie and G. Gottstein: Z. Metallk., vol.71, 1980, pp. 279-285.
- [6] G. Gottstein and U.F. Kocks: Acta Met., vol. 31, 1983, pp. 175-188.
- [7] M.J. Luton and C.M. Sellars : Acta Met., vol. 17, 1969, pp. 1033-1043.
- [8] A.A. Guimaraes and J.J. Jonas: Met. Trans., vol. 12A, 1981, pp. 1655-1667.
- [9] D.R. Barraclough and C.M. Sellars : Met. Sci., vol. 13, 1979, pp. 257-267.
- [10] L.C. Lim and R. Raj : Acta Met., vol. 33, 1985, pp.2205-2214.
- [11] R.E. Cook, G. Gottstein and U.F. Kocks : J. Mat. Sci., vol. 18, 1983, pp. 2650-2664.
- [12] B.S. Majumdar and S.J. Burns : Acta Met., vol. 30, 1982, pp. 1751-1760
- [13] H. Nahm, J. Moteff and D.R. Dierks: Acta Met., vol. 25, 1977, pp. 107-116.

- [14] A.M. Ermi and J. Moteff: Met. Trans., 13A, 1982, pp. 1577-1588.
- [15] A.M. Ermi and J. Moteff: J. Eng. Mat. Tech., vol. 105, 1983, pp. 21-30.
- [16] J.C. Figueroa, S.P. Bhat, R.De La Veaux, S. Murzenski and C. Laird
 : Acta Met., vol. 29, 1981, pp. 1667-1678.
- [17] T. Ito, T. Taketani and Y. Nakayama: Scripta Met., vol. 20, 1986, pp. 1329-1332.
- [18] T.G. Langdon and R.C. Gifkins: Acta Met., vol. 31, 1983, pp. 927-938.
- [19] T.G. Langdon, D. Simpson and R.C. Gifkins: Acta Met., vol. 31, 1983, pp. 939-946.
- [20] P. Yavari and T.G. Langdon: Acta Met., vol. 31, 1983, pp. 1595-1603.
- [21] P. Yavari and T.G. Langdon: Acta Met., vol. 31, 1983, pp. 1605-1610.
- [22] H. Abdel-Raouf, A. Plumtree and T.H. Topper: Metall. Trans., vol. 5, 1974, pp. 267-277.
- [23] H. Mecking and G. Gottstein, in "Recrystallization of Metallic Materials" (edited by F. Haessner), 2nd edn., pp. 195-222, Dr. Riederer Verlag, Stuttgart, 1978.
- [24] G. Gottstein, D. Zabardjadi and H. Mecking: Metal Sci., vol. 13, 1979, pp. 223-227.
- [25] T. Hasegawa and U.F. Kocks: Acta met., vol. 27, 1979, p. 1705.
- [26] T. Sakai and J.J. Jonas: Acta Met., vol. 32, 1984, pp. 189-209.
- [27] C. Rossard: Metaux, vol. 35, 1960, pp. 102-115, 140-153, 190-205.
- [28] L.F. Coffin Jr.: J. Mat., vol. 6, 1971, p. 388.

- [29] L.F. Coffin Jr., S.S. Manson, A.E. Carden, L.K. Serverud and W.L. Greenstreet: "The Dependent Fatigue of Structural Alloys, A General Assessment", 1975, ORNL-5073, Published Jan. 1977.
- [30] S.S. Manson: "Fatigue at Elevated Temperature", ASTM STP 520, 1973, p. 744.
- [31] D.R. Dierks: "Advances in Design for Elevated Temperature Environment", ASME 1975, p. 29.
- [32] H. Mughrabi in "Strength of Metals and Alloys", eds. P. Haasen,V. Gerold and G. Kostorz, Pergamon Press, 1980, p. 1615.
- [33] L.M. Brown: Met. Sci., vol. 11, 1977, p. 315.
- [34] S.J. Basinski, Z.S. Basinski and A.W. Howe: Phil. Mag., vol. 19, 1969, p. 899.
- [35] G. Konig and W. Blum: Acta Met., vol. 28, p. 1467.
- [36] G.E. Dieter: "Mechanical Metallurgy", 2nd edn., McGraw-Hill, Inc., 1976, p. 396.
- [37] E. Furubayashi and M. Nakamura: Proc. ICOTOM 6, p. 619, Iron Steel Inst. Japan, Tokyo, 1981.
- [38] H.J. McQueen and J.J. Jonas, in "Recovery and Recrystallization during High Temperature Deformation" in Treatise on Materials Science and Technology, vol. 6, 1975, pp. 393-493.
- [39] V. Raman and T.C. Reiley: Scripta Met., vol. 20, 1986, pp. 1343-1346.
- [40] S.P. Bhat and C. Laird: Int. J. Fatigue Engng. Mater. Struct., vol. 1, 1979, pp. 59-77.
- [41] S.P. Bhat and C. Laird: Int. J. Fatigue Engng. Mater. Struct., vol. 1, 1979, pp. 79-92.